

Splitting Dioxygen over Distant Binuclear Fe Sites in Zeolites. Effect of the Local Arrangement and Framework Topology

Edyta Tabor, Mariia Lemishka, Joanna E. Olszowka, Kinga Mlekodaj, Jiri Dedecek, Prokopis C. Andrikopoulos, and Stepan Sklenak*



Cite This: *ACS Catal.* 2021, 11, 2340–2355



Read Online

ACCESS |

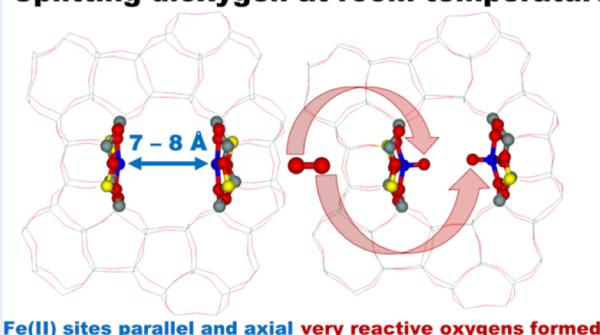
Metrics & More

Article Recommendations

ABSTRACT: Activation of dioxygen is of extreme importance due to its potential for transformation of methane to valuable products and applications in other selective oxidation reactions. Distant binuclear cationic Fe(II) centers in Fe-ferrierite were shown to split dioxygen at room temperature to form a pair of very active oxygen species (i.e., α -oxygens) and subsequently oxidize methane to methanol at room temperature as well. Our study reveals that the activity in splitting dioxygen represents a general property of the distant binuclear cationic Fe(II) centers stabilized in the aluminosilicate matrix. Computational models of the ferrierite, beta, A, and mordenite zeolites with various Al sitings in the rings forming the cationic sites were investigated by periodic DFT calculations including molecular dynamics simulations. The results reveal that the Fe(II) sites stabilized in various zeolite matrices can split dioxygen if the two cationic sites forming the distant binuclear Fe(II) centers (i) face each other, (ii) are parallel, and (iii) are axial, and (iv) the Fe...Fe distance lies in a narrow range from ca. 7 to ca. 8 Å (ca. 7–ca. 10 Å for the distance between the two rings (forming the corresponding cationic sites) in empty zeolites since this distance is equal to or larger than the Fe...Fe distances). Our study opens the possibility of developing Fe-zeolite-based systems for the dioxygen activation employed for direct oxidations using various zeolite matrices.

KEYWORDS: *alpha oxygen, oxidation of methane, utilization of methane, selective oxidation of hydrocarbons, direct oxidation of hydrocarbons, transition metal-exchanged zeolites, density functional theory, ferrierite, beta zeolite*

Splitting dioxygen at room temperature



Fe(II) sites parallel and axial very reactive oxygens formed

1. INTRODUCTION

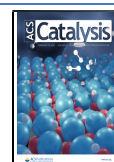
Activation of dioxygen for its employment as an abundant, eco-friendly, and low-cost oxidant represents one of the greatest challenges in oxidation catalysis.^{1–4} Naturally occurring systems are able to activate dioxygen for direct oxidation reactions over metalloenzymes, for example, oxidation of methane to methanol over methane monooxygenase.⁵ Mastering the activation of dioxygen, especially for utilization of methane to produce valuable products on an industrial scale, is highly desirable. Methane represents the dominant component of natural and shale gases, and its transformation to liquid valuable products such as methanol is in high demand. Currently, processing methane into the required products is energetically, technologically, and investably very demanding. Methane is transformed into synthesis gas (H_2 and CO) which is subsequently either catalytically converted to methanol or by Fischer–Tropsch synthesis processed into liquid hydrocarbons.⁶ Thus, a direct route of oxidation of methane to methanol would represent a huge leap forward in methane utilization if employing a cheap oxidant such as dioxygen.

Recently, intensive research in this area has been focused on the activity of Fe and Cu cations and oxide clusters stabilized in aluminosilicate matrices of zeolites. In this case, methanol is produced by direct methane oxidation in a three-step reaction process consisting of (i) oxidative activation, (ii) methane reaction, and (iii) steam-aided methanol desorption. A subsequent regeneration by oxidative treatment of the Cu-zeolite usually restores the activity, as can be seen in reports of the reaction with multiple cycles.^{7,8} The oxidative activation of the catalyst is an important bottleneck for the continuous production of methanol via methane oxidation on Cu-zeolites.⁸ At the present time, the reported systems provide methanol yields per gram of the catalyst up to 200 $\mu\text{mol g}^{-1}$ in a single

Received: October 14, 2020

Revised: January 20, 2021

Published: February 5, 2021



reactive cycle.⁹ Nevertheless, the highest values of the methanol yield per cycle are reached for (i) cycles lasting for hours and (ii) changing operation temperatures typically from ca. 180–200 °C for the methane oxidation and/or methanol release and 400–450 °C for the formation of Cu-oxo species. Although the production of methanol per gram of the catalysts or copper is an important parameter which provides the information on the activity of the Cu centers and their concentration in the zeolite matrix, the time-related activity of the catalysts (the yield of methanol per gram of the catalyst per hour) is the key parameter from the point of view of the production process. In this case, long-time cycles for methanol production with variations of temperature do not provide significant yields. Although a marked improvement has been reached and an isothermal process of the oxidation of methane over Cu-zeolites has been developed, the yields obtained are too low to be promising for industrial application as they show a very low methanol productivity (2.6–3.3 mg_{CH₃OH} g_{catalyst}⁻¹ h⁻¹).^{2,3,10–13} The continuous direct conversion of CH₄ to CH₃OH on Cu-based catalysts has only been achieved even with lower methanol yields (60–520 μg_{CH₃OH} g_{catalyst}⁻¹ h⁻¹).^{2,8,14} Therefore, the currently reported systems can be regarded as unrealistic or at least unpromising as the base for the technology of methane utilization.¹⁵ The previously discovered activity¹⁶ regarding the direct oxidation of methane to methanol over isolated Fe cations stabilized in zeolite matrices by the α -oxygen formed by the decomposition of N₂O does not represent a real basis for a possible technological application of the production of methanol from methane either as the price of N₂O is higher than that of methanol.^{5,17,18} Thus, there is plenty of room for improvements of the catalysts. Moreover, there is a significant need of new reaction systems enabling the isothermal oxidation of methane and not requiring the assistance of water or the water–organic medium for the extraction of methoxy groups strongly bound to the catalyst.

Very recently, a breakthrough¹⁹ in the dioxygen activation has been achieved.⁴ Two cooperating distant Fe cations stabilized in Fe-zeolite of the ferrierite topology (FER) undergo an Fe(II) → Fe(IV) redox cycle. The distant binuclear cationic Fe(II) centers in Fe-ferrierite are, on the one hand, close enough to cooperate in a four-electron process of dioxygen activation but, on the other hand, far enough that a formation of an oxo-bridge species known for metalloenzymes^{4,5} is not possible and splitting dioxygen occurs even at room temperature.⁴ The cleavage of dioxygen results in the formation of a pair of very active oxygen species called the α -oxygen (i.e., [Fe(IV)=O]²⁺).^{1,4,20–22} The α -oxygen on isolated Fe cations is known for its exceptional properties regarding the direct oxidation of methane to methanol^{16,23} and benzene to phenol.^{24,25} However, until now, it has been possible to prepare the α -oxygen exclusively by the abstraction of the oxygen atom from N₂O over isolated iron species in ZSM-5,^{16,23–26} ferrierite,^{20–22} SSZ-13,²⁷ and the beta zeolite.^{1,26} The unique oxidation properties concerning the direct oxidation of methane to methanol at room temperature were recently confirmed also for a pair of the α -oxygen atoms prepared by splitting dioxygen over the distant binuclear Fe(II) sites stabilized in the ferrierite matrix.⁴ These oxidized centers when employed for the direct oxidation of methane to methanol feature an additional advantage that is an easy release of the oxidation products from the system without the necessity of water or water–organic medium extraction of the

oxidation products.^{4,22} These results make the distant binuclear Fe(II) sites stabilized in a zeolite matrix a highly promising material for the direct methane oxidation.^{4,22}

The DFT-calculated barriers of splitting dioxygen (25 kcal/mol)⁴ and abstracting oxygen from N₂O (15 kcal/mol)²² over Fe-ferrierite reveal facile oxidations of the Fe(II) cations of Fe-ferrierite to yield the α -oxygen. However, there is a question whether the low barriers result from the unique topology of the ferrierite zeolite and the Al organization²⁸ (especially the Al siting in the rings forming the cationic sites) in the ferrierite used or if the activity regarding splitting dioxygen represents a general property of the distant binuclear Fe(II) centers stabilized in the aluminosilicate matrix. If the latter is true, it can represent a highly promising base for the development of exceptionally active systems with higher concentrations of the active sites for the direct oxidation of methane. Moreover, splitting dioxygen over the distant binuclear Fe(II) centers located at the opposite sides of the wall of larger channels potentially opens the possibility of using the α -oxygen atoms also for the direct oxidation of bulkier molecules with a restricted access to the α -oxygen atoms through eight-rings (i.e., via the ferrierite side channel).

The activity in splitting dioxygen of the distant binuclear Fe(II) centers in zeolites can be, in general, affected by a number of structural parameters, for example, the distance of the rings accommodating Fe(II) and their mutual geometrical position (i.e., facing or not facing each other, parallel or nonparallel, and if parallel, whether axial or nonaxial). However, also the local arrangement of Fe(II) in the cationic sites may play a role. This local arrangement is^{4,21,22,29,30} not given only by the structure of the zeolite ring accommodating Fe(II) but also by the Al siting in this ring.²⁸ We have shown that the formation of the distant binuclear M(II) cationic centers in zeolites requires fulfilling three conditions:^{4,22} (i) The presence of two rings able to form close cationic sites for bare divalent cations. The two rings must face each other. (ii) Each of the two rings has to contain two Al atoms (four Al atoms in total, i.e., two Al pairs²⁸). (iii) The two cationic sites must be occupied by two divalent cations.

The availability of zeolite matrices with suitable Al organizations^{28,31,32} required for the stabilization of high concentrations of the distant binuclear Fe(II) sites is essential to answer the questions regarding the uniqueness of the ferrierite topology and concerning the effects of (i) the Al siting in the rings forming the cationic sites, (ii) the distance, and (iii) the mutual geometrical position of the rings accommodating Fe(II) on the activity of the distant binuclear Fe(II) sites in dioxygen splitting. The known Al organizations for the topologies used for our investigation are discussed below.^{28,31,32}

The activity in splitting dioxygen was proven for the distant binuclear Fe sites formed by two Fe(II) cations located in the adjacent β cationic sites of ferrierite. Al pairs forming these β cationic site are created only by the Al(T2)–Si–Si–Al(T2) sequences (i.e., β_2 ^{21,29,33}).^{31–33} Their ability to form the distant binuclear active sites able to split dioxygen has already been confirmed.⁴ There have been no reports that the β cationic site in ferrierite is composed of Al(T4)–Si–Si–Al(T4) sequences (i.e., β_1 ^{21,29,33}) to the best of our knowledge.

The Si/Al ratio of the ferrierite sample used in our previous study²¹ (Tosoh Corporation, Japan) is 8.6, implying that there are, in average, 3.75 Al atoms per unit cell. The previous

investigation revealed that the concentration of Al pairs in the α site is low (10% of all the Al atoms),^{21,33} so only a very small fraction of the α sites are able to form binuclear Fe(II) structures. It should be noted that other ferrierites exhibit similar Al distributions at best.^{31,32} Some ferrierite matrices feature significantly lower concentrations of Al pairs.^{31,32}

A total of 25% of all the Al atoms in mordenite with Si/Al 8.8 form the β cationic site.^{31,32,34} However, the Al siting in the rings forming the β sites is not known, and therefore, mordenite cannot be employed to experimentally study the effect of the Al organization on splitting dioxygen.

Our prior study of beta zeolites showed that, in maximum, ca. 30–40% of all the Al atoms created the β cationic site.³⁵ However, it should be noted that there are four double six-rings, each forming two possible β cationic sites per unit cell, and only four of the β cationic sites are located at the opposite sides of the wall of the 12-ring channel. Therefore, only a smaller fraction of the β sites are able to form binuclear Fe(II) structures even in Al-rich beta zeolites.^{31,32,35}

Recently, a significant step ahead in the development of methods allowing the control of the Al organization in zeolites has been made.^{31,32,36} However, it should be noted that syntheses of zeolites of different topologies with the controlled Al organization would require a long-term highly complex and demanding research. This clearly evidences that a computational approach represents the only way permitting to answer the questions raised above.

In this article, we use periodic DFT calculations to investigate the effect of (i) the Al siting in the rings forming the cationic sites, (ii) the distance, and (iii) the mutual geometrical position of the rings accommodating Fe(II) on the activity of the distant binuclear Fe(II) sites in splitting dioxygen. The ferrierite, mordenite, beta, and A zeolites were employed for this purpose. The obtained results clearly evidence that the capability of splitting dioxygen is general for the distant binuclear Fe(II) sites with suitable parameters. This result suggests the possibility of developing highly active tunable systems capable of splitting dioxygen. Such substances represent a base for the development of materials for the direct oxidation of methane or even bulkier molecules.

2. COMPUTATIONAL MODELS AND METHODS

2.1. Computational Models. Seven models with the P1 symmetry are used for the distant binuclear Fe(II) centers located in various cationic sites of four zeolites. The FER_{aaa} and FER _{$\beta_1\beta_1$} models employ one and two (along the *c* dimension), respectively, unit cells of ferrierite and feature two Fe(II) cations located in two adjacent α ^{21,29,33} and β_1 ,^{21,29,33} respectively, cationic sites. The BEA _{$\beta_{T5\beta T6}$} and BEA _{$\beta_{T7\beta T8}$} models use two (along the *b* dimension) unit cells of the beta zeolite and contain two Fe(II) cations accommodated in two β cationic sites³⁵ facing each other across the 12-ring channel. Two different Al sitings in the six-rings forming the β cationic sites are used: (i) Al(T5), Al(T5), Al(T6), and Al(T6) for the BEA _{$\beta_{T5\beta T6}$} model and (ii) Al(T7), Al(T7), Al(T8), and Al(T8) for the BEA _{$\beta_{T7\beta T8}$} model. The LTA model uses two unit cells of the A zeolite and includes two Fe(II) cations accommodated in two adjacent six-rings. It should be noted that LTA is only a model structure featuring two adjacent cationic sites which are not parallel, and therefore, only two Al atoms in each of the six-rings are used. The MOR _{$\beta_{T1\beta T1}$} and MOR _{$\beta_{T3\beta T3}$} models employ two (along the *c* dimension) unit cells of mordenite and incorporate two Fe(II)

cations bound in two adjacent β cationic sites.³⁴ Al(T1)–Si(T1)–Si(T3)–Si(T3)–Al(T1) and Al(T3)–Si(T3)–Si(T1)–Si(T1)–Al(T3) sequences in the eight-rings forming the β cationic sites are employed in the MOR _{$\beta_{T1\beta T1}$} and MOR _{$\beta_{T3\beta T3}$} , respectively, models. The MOR models based on the other possible Al sitings in the eight-ring are not used since our calculations reveal that either the Fe cations are coordinated in a different ring or the coordination of the Fe(II) cations is pseudo-tetrahedral with a closed coordination sphere and therefore not meeting experimentally observed spectra of Co(II) cations in this site.³⁴

The starting geometries of FER_{aaa}, FER _{$\beta_1\beta_1$} , BEA _{$\beta_{T5\beta T6}$} , BEA _{$\beta_{T7\beta T8}$} , LTA, MOR _{$\beta_{T1\beta T1}$} , and MOR _{$\beta_{T3\beta T3}$} are generated from the experimental structures of the corresponding zeolites. FER_{aaa} and FER _{$\beta_1\beta_1$} : orthorhombic, space group *Immm*, and cell parameters *a* = 18.651, *b* = 14.173, and *c* = 7.404 Å;³⁷ BEA _{$\beta_{T5\beta T6}$} and BEA _{$\beta_{T7\beta T8}$} : polymorph A of the beta zeolite, tetragonal, space group *P4₂2₂*, and cell parameters *a* = *b* = 12.6320 and *c* = 26.1860 Å;³⁸ LTA: cubic, space group *Pm3m*, and cell parameters *a* = *b* = *c* = 11.9190 Å;³⁸ MOR _{$\beta_{T1\beta T1}$} and MOR _{$\beta_{T3\beta T3}$} : orthorhombic, space group *Cmcm*, and cell parameters *a* = 18.2560, *b* = 20.5340, and *c* = 7.5420 Å.³⁸

2.2. Electronic Structure Calculations. Periodic DFT calculations were performed by employing the Vienna Ab initio Simulation Package (VASP) code.^{39–42} The high-spin electron configuration $d5\uparrow d1\downarrow$ was used for the Fe species accommodated in the zeolite.⁴ Moreover, for all the calculated optimized structures for all of the seven computational models, the electron configuration used was verified that it really corresponds to the ground state.⁴ The Kohn–Sham equations were solved variationally in a plane-wave basis set using the projector-augmented wave method of Blöchl,⁴³ as adapted by Kresse and Joubert.⁴⁴ The exchange–correlation energy was described by the Perdew–Burke–Ernzerhof⁴⁵ (PBE) generalized gradient approximation functional. Brillouin zone sampling was restricted to the Γ point.⁴ A plane-wave cutoff of 600 eV and the density-dependent energy correction (dDsC) dispersion correction^{46,47} were used for the geometry optimizations, and a smaller cutoff of 400 eV and the DFT-D2 method⁴⁸ were used for the molecular dynamics (MD) simulations.⁴

2.3. Molecular Dynamics. MD simulations were carried out on the seven models. The MD computations used the exact Hellmann–Feynman forces acting on atoms and applied the statistics of the canonical ensemble to the motion of the atomic nuclei⁴⁹ using the Verlet velocity algorithm^{50,51} to integrate Newton's equations of motion. The time step for the integration of the equations of motion was 1 fs.⁴ The simulations were run for 10,000 fs at 400 K.⁴ Visual inspection of the structures along the MD trajectories showed that the duration of the MD simulations was long enough because it included both the rearrangements of the local structures of the ferrierite framework (up to ca. 2000 fs) and a long period (ca. 8000 fs) when the system fluctuated around the equilibrium and “snapshots” were collected and optimized. Similar time lengths were used for MD simulations of cationic sites in zeolites.^{4,22,30,52,53} The MD simulations serve to obtain the rearranged local structures (details are provided in our prior studies^{21,29}). The structures of 20 distinct snapshots collected at 500, 1000, 1500, ... 10,000 fs of the MD simulations were optimized for the seven computational models.⁴

2.4. Geometry Optimizations. The collected snapshots were optimized. The atomic positions were optimized at

Table 1. Stabilization Energies^a (ΔE) in kcal/mol of the Cationic Sites Accommodating Fe(II) for the Seven Models

FER _{$\alpha\alpha$}	FER _{$\beta_1\beta_1$}	BEA _{$\beta_{T5}\beta_{T6}$}	BEA _{$\beta_{T7}\beta_{T8}$}	LTA	MOR _{$\beta_{T1}\beta_{T1}$}	MOR _{$\beta_{T3}\beta_{T3}$}
12.3	0.4	3.9	1.2	0.8	11.0	2.6

^aThe difference between the energies of the model relaxed by MD simulations and subsequently optimized and the model which was not relaxed by MD simulations but simply optimized using the starting structure.

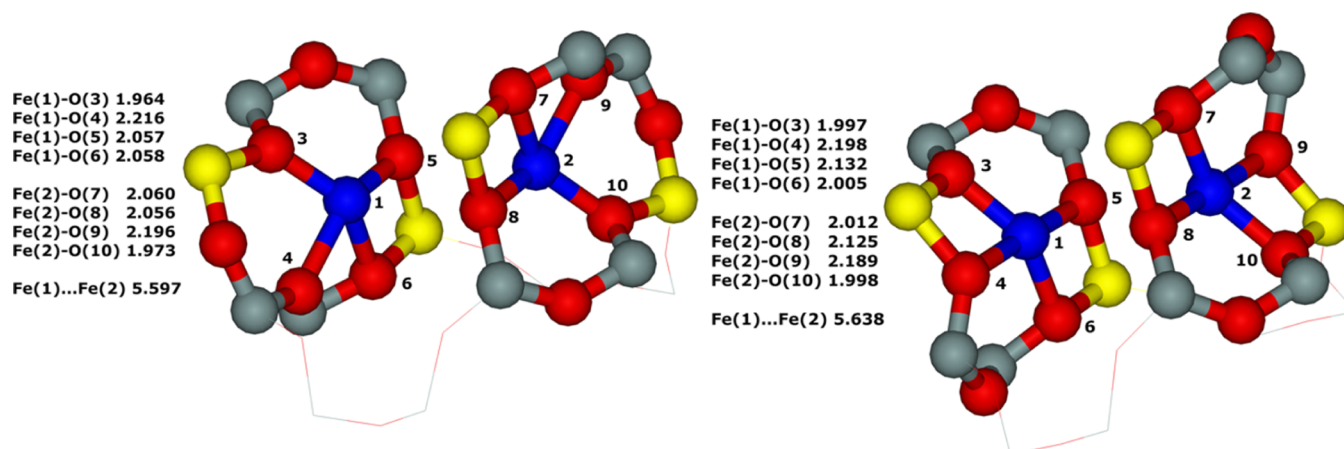


Figure 1. Optimized structures of ferrierite before (left) and after (right) the DFT molecular dynamics simulations for two adjacent α (FER _{$\alpha\alpha$} model) sites. The distances are in Å. Silicon atoms are in gray, aluminum atoms are in yellow, iron atoms are in blue, and oxygen atoms are in red.

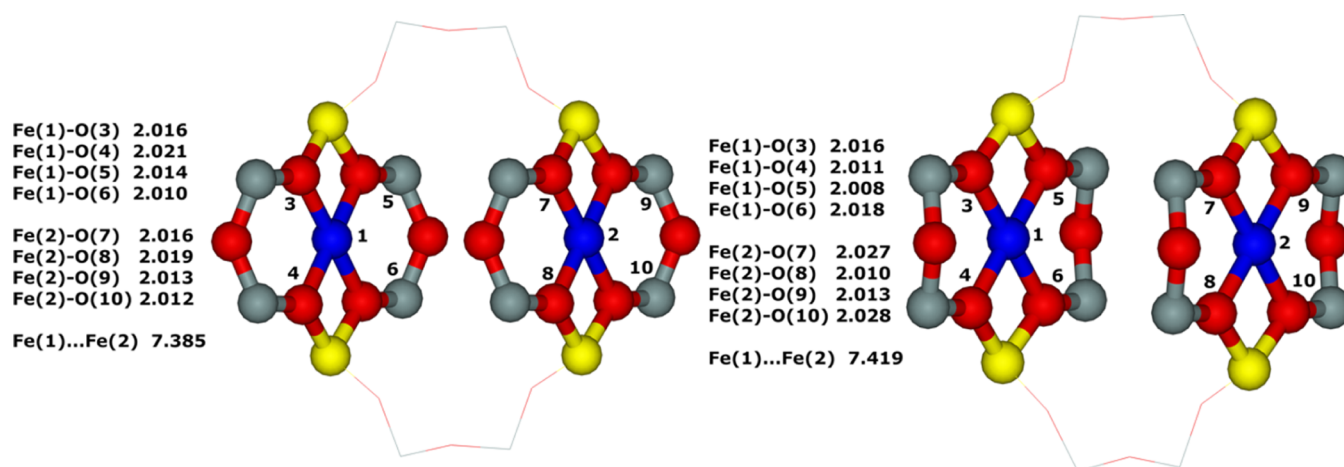


Figure 2. Optimized structures of ferrierite before (left) and after (right) the DFT molecular dynamics simulations for two adjacent β_1 (FER _{$\beta_1\beta_1$} model) sites. The distances are in Å. Silicon atoms are in gray, aluminum atoms are in yellow, iron atoms are in blue, and oxygen atoms are in red.

constant volume using a conjugate-gradient algorithm minimization of energies and forces, whereas the lattice parameters were fixed at their experimental values.⁴ The most stable structure for each of the seven investigated models was then used for the subsequent calculations of all the complexes, transition states, and products.

In addition, all the seven models were optimized using the starting geometries without employing MD simulations. Ten different starting positions of the Fe(II) cations were used for each of the models. The most stable structure for each of the seven investigated models was employed for evaluating the stabilization energies.

3. RESULTS

3.1. Structure and Stability of the Fe(II) Cationic Sites. Our MD simulations of the seven models and subsequent optimizations of the selected MD snapshots led to energy stabilizations relative to the seven models which were

not relaxed by employing MD simulations but simply optimized using the starting geometries. The stabilization is significant for the MOR _{$\beta_{T1}\beta_{T1}$} and FER _{$\alpha\alpha$} models, while it is moderate for the remaining five models (Table 1).

3.1.1. FER _{$\alpha\alpha$} and FER _{$\beta_1\beta_1$} Models. The optimized structures before and after the MD calculations are shown in Figures 1 and 2, respectively.

The FER _{$\alpha\alpha$} model significantly rearranges ($\Delta E = 12$ kcal/mol), while the FER _{$\beta_1\beta_1$} model is almost unchanged by the MD calculations. The Fe(II) cations in the former coordinate to three oxygen atoms of two AlO₄⁻ tetrahedra and one oxygen atom of an SiO₄ tetrahedron before the rearrangement, and only after the rearrangement, this model features the proper^{21,29} coordination of Fe(II) to four oxygen atoms of two AlO₄⁻ tetrahedra (Figure 1). Conversely, the Fe(II) cations in the latter possess the proper coordination to four oxygen atoms of two AlO₄⁻ tetrahedra before and after the MD calculations (Figure 2).

Table 2. Mutual Geometrical Position of the Two Cationic Sites, $\text{Fe}\cdots\text{Fe}^a$ and Two Ring^b Distances, Barrier ΔE_{ACT1} ,^c Reaction Energy ΔE_{R} ,^d Reverse Barrier ΔE_{ACT2} ,^e and $\Delta\Delta E_{\text{ACT}}$ (i.e., $\Delta E_{\text{ACT2}} - \Delta E_{\text{ACT1}}$)

model	facing ^f	parallel	axial	Fe \cdots Fe (Å)	ring \cdots ring (Å)	ΔE_{ACT1} (kcal/mol)	ΔE_{R} (kcal/mol)	ΔE_{ACT2} (kcal/mol)	$\Delta\Delta E_{\text{ACT}}$ (kcal/mol)
FER $_{\alpha\alpha}$	yes	yes	yes	5.638	6.5				
FER $_{\beta1\beta1}$	yes	yes	yes	7.419	7.4	21.3	-23.3	23.7	2.4
FER $_{\beta2\beta2}$ ^g	yes	yes	yes	7.405	7.4	24.9	-24.7	28.0	3.1
BEA $_{\beta\text{T5}\beta\text{T6}}$	yes	yes	yes	7.627	9.5	31.4	-33.0	39.2	7.8
BEA $_{\beta\text{T7}\beta\text{T8}}$	yes	yes	yes	7.611	9.5	31.2	-32.6	36.4	5.2
LTA	yes	no		7.327	7.6	61.6	-27.7	62.4	0.8
MOR $_{\beta\text{T1}\beta\text{T1}}$	yes	yes	yes	7.261	7.5	15.0	-19.2	22.9	7.9
MOR $_{\beta\text{T3}\beta\text{T3}}$	yes	yes	no	7.550	7.5				

^aThe Fe \cdots Fe distance after the MD simulations. ^bThe distance between the two rings (forming the corresponding cationic sites) in empty zeolites derived from results of diffraction experiments. ^cThe calculated barrier of the cleavage of dioxygen. ^dThe reaction energy of the reaction from 1 + O₂(g) to give 4. ^eThe calculated barrier of the recombination of dioxygen (i.e., 4 to yield 3). ^fWhether facing each other. ^gThe data for the FER $_{\beta2\beta2}$ model are taken from our prior study.⁴

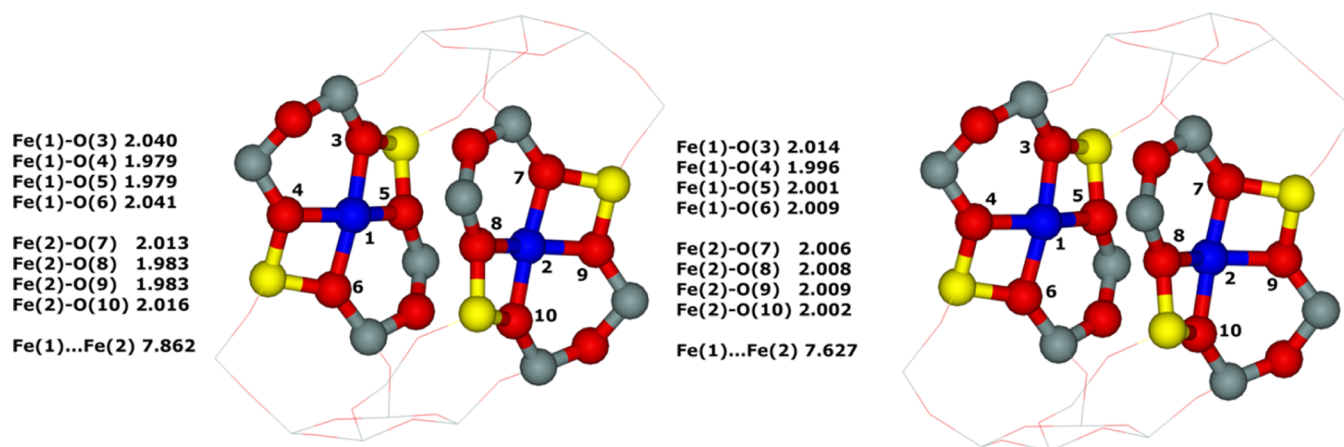


Figure 3. Optimized structures of the beta zeolite before (left) and after (right) the DFT molecular dynamics simulations for two opposite βT5 and βT6 (BEA $_{\beta\text{T5}\beta\text{T6}}$ model) sites across the 12-ring channel. The distances are in Å. Silicon atoms are in gray, aluminum atoms are in yellow, iron atoms are in blue, and oxygen atoms are in red.

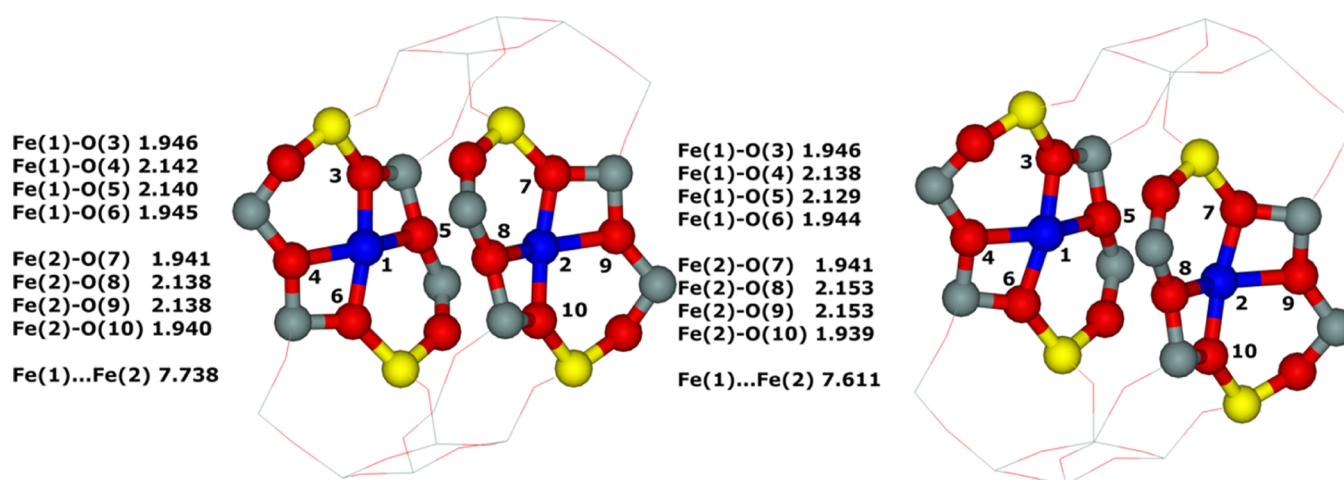


Figure 4. Optimized structures of the beta zeolite before (left) and after (right) the DFT molecular dynamics simulations for two opposite βT7 and βT8 (BEA $_{\beta\text{T7}\beta\text{T8}}$ model) sites across the 12-ring channel. The distances are in Å. Silicon atoms are in gray, aluminum atoms are in yellow, iron atoms are in blue, and oxygen atoms are in red.

α Cationic sites of ferrierite are located on the wall of the 10-ring main channel. Two adjacent α cationic sites (FER $_{\alpha\alpha}$) are located at the opposite sides of the wall of the main channel. The mutual geometrical position of the two cationic sites (i.e., facing or not facing each other, parallel or nonparallel, and if parallel, whether axial or nonaxial) and the corresponding Fe \cdots

Fe distance after the MD calculations are summarized in Table 2. β Cationic sites of ferrierite are present on the wall of the eight-ring channel. Two adjacent $\beta1$ cationic sites (FER $_{\beta1\beta1}$) are present at the opposite sides of the wall of the eight-ring channel. The mutual geometrical position of the two cationic sites and the Fe \cdots Fe distance are shown in Table 2. The Fe–O

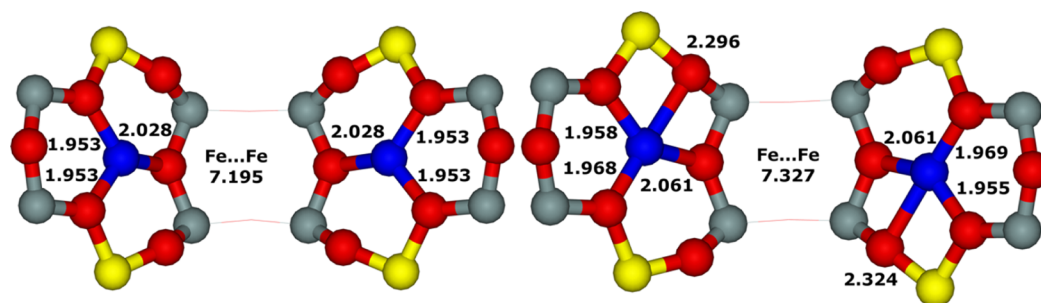


Figure 5. Optimized structures of the A zeolite before (left) and after (right) the DFT molecular dynamics simulations for two adjacent six-ring (LTA model) sites. The distances are in Å. Silicon atoms are in gray, aluminum atoms are in yellow, iron atoms are in blue, and oxygen atoms are in red.

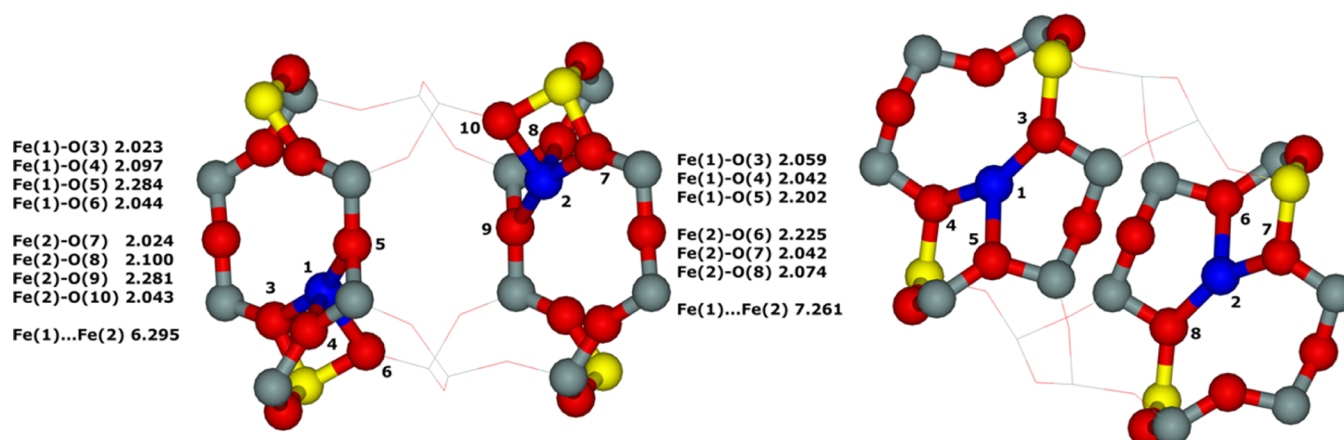


Figure 6. Optimized structures of mordenite before (left) and after (right) the DFT molecular dynamics simulations for two adjacent β T1 ($MOR_{\beta T1/\beta T1}$ model) sites. The distances are in Å. Silicon atoms are in gray, aluminum atoms are in yellow, iron atoms are in blue, and oxygen atoms are in red.

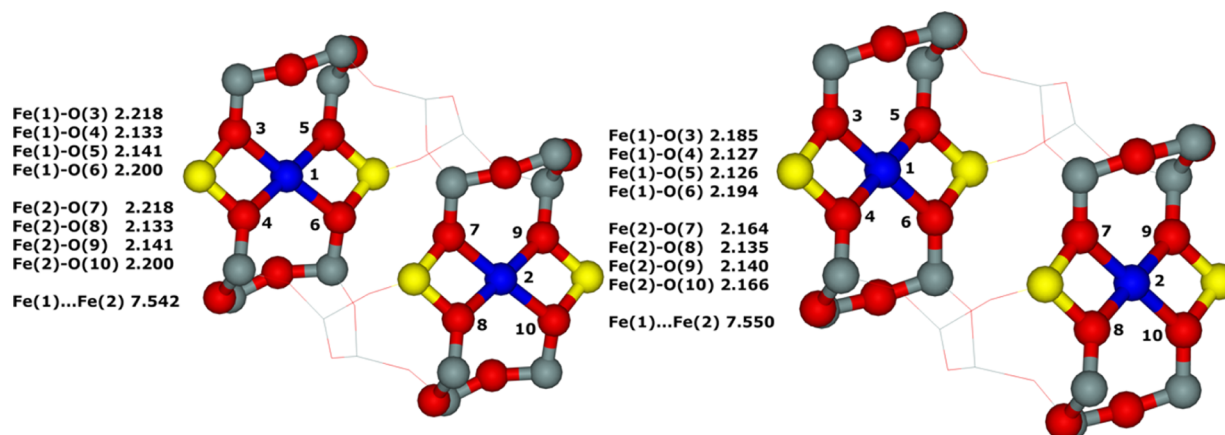


Figure 7. Optimized structures of mordenite before (left) and after (right) the DFT molecular dynamics simulations for two adjacent β T3 ($MOR_{\beta T3/\beta T3}$ model) sites. The distances are in Å. Silicon atoms are in gray, aluminum atoms are in yellow, iron atoms are in blue, and oxygen atoms are in red.

bond lengths in FER_{α} (Figure 1) optimized after the MD simulations range from 2.00 to 2.20 Å (four Fe–O bonds are shorter than the other four), while all the eight Fe–O bond lengths are almost identical (2.01 to 2.03 Å) in $FER_{\beta 1/\beta 1}$ (Figure 2).

3.1.2. $BEA_{\beta T5/\beta T6}$ and $BEA_{\beta T7/\beta T8}$ Models. The optimized structures before and after the MD calculations are shown in Figures 3 and 4, respectively.

Both the models of the beta zeolite moderately rearrange ($\Delta E = 1\text{--}4$ kcal/mol), and only the $BEA_{\beta T5/\beta T6}$ model possesses the proper^{21,29} coordination of Fe(II) to four oxygen atoms of two AlO_4^- tetrahedra before and after the MD calculations. Conversely, Fe(II) in $BEA_{\beta T7/\beta T8}$ ligates to two O atoms of two AlO_4^- tetrahedra and two O atoms of two SiO_4 tetrahedra before and after the MD calculations. The same results were obtained for Co(II)-exchanged beta zeolites in our prior study.³⁵ The reason why the $BEA_{\beta T7/\beta T8}$ model does not

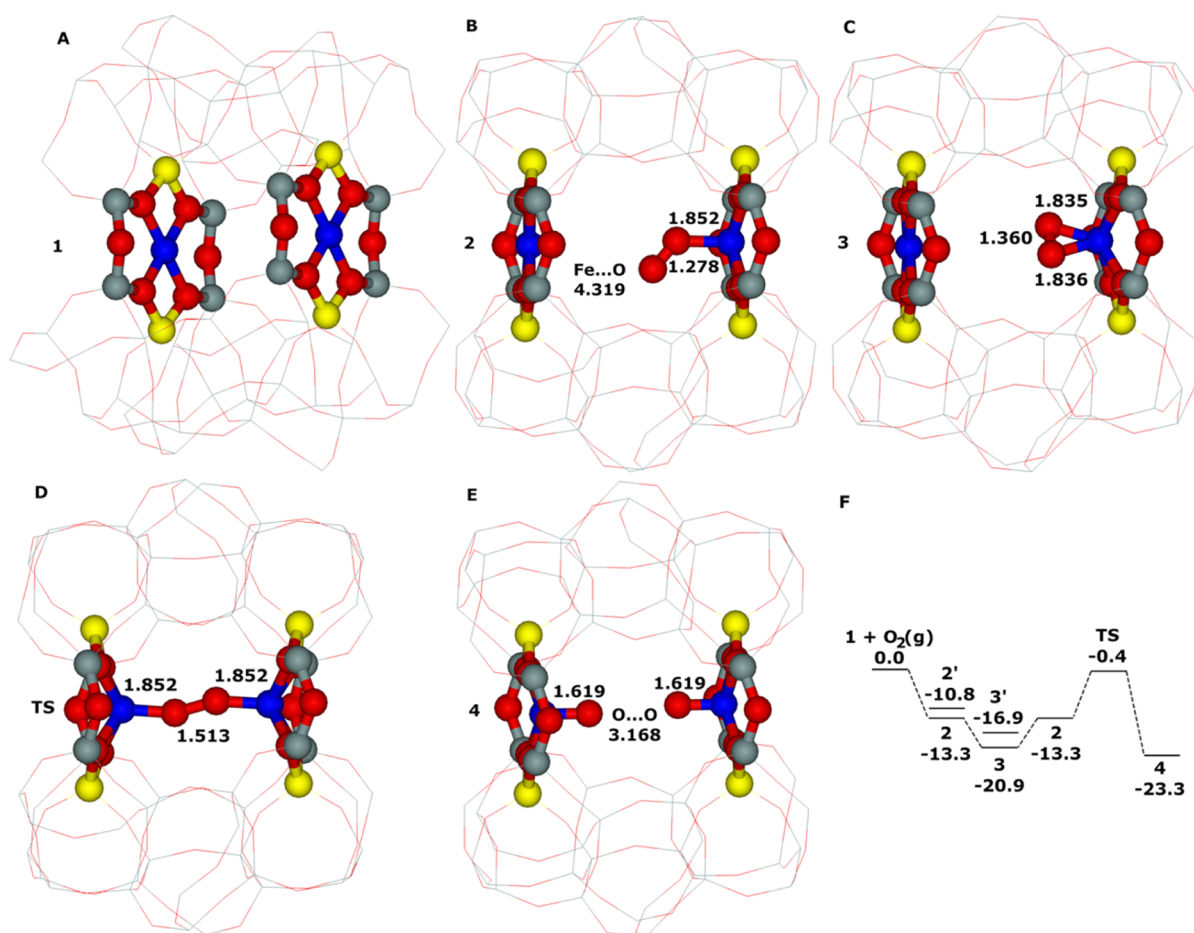


Figure 8. FER _{β 1} model. Optimized structures for the (A) two adjacent β 1 sites of Fe-ferrierite 1 after molecular dynamics (MD) simulations, (B) monodentate [Fe OO_{mono}...Fe] complex 2, (C) bidentate [Fe OO_{bi}...Fe] complex 3, (D) [Fe–O–O–Fe] transition state TS, and (E) [Fe=O O=Fe] product 4. The distances are in Å. Silicon atoms are in gray, oxygen atoms are in red, aluminum atoms are in yellow, and iron atoms are in blue. Schematic energy profile (in kilocalorie per mol) for (F) the formation of the Fe=O O=Fe product 4.

rearrange in order for Fe(II) to bind to four O atoms of two AlO_4^- tetrahedra, most likely, is that the six-rings forming β T5 and β T6 cationic sites create a rigid double six-ring (i.e., hexagonal prism) with another six-ring. The stabilization energy obtained from the proper binding of Fe(II) to four O atoms of two AlO_4^- tetrahedra is most likely smaller than the energy needed to deform the structure of the double six-ring to permit the proper binding of Fe(II).

β Cationic sites of the beta zeolite are located on the wall of the 12-ring channel. Two opposite β cationic sites (β T5 and β T6 of BEA _{β T5 β T6 and β T7 and β T8 of BEA _{β T7 β T8) are present at the opposite sides of the wall of the 12-ring channel. The mutual geometrical position of the two cationic sites and the Fe...Fe distance are shown in Table 2. All the Fe–O_{Al} bond lengths of the BEA _{β T5 β T6 model (Figure 3) are almost identical (2.00–2.01 Å), while the Fe–O_{Al} bonds are significantly shorter (1.94–1.95 Å) than the Fe–O_{Si} bonds (2.13–2.15 Å) in the BEA _{β T7 β T8 model (Figure 4).}}}}

3.1.3. LTA Model. The optimized structures before and after the MD calculations are shown in Figure 5.

The Fe(II) cations coordinate to two oxygen atoms of two AlO_4^- tetrahedra and one oxygen atom of an SiO_4 tetrahedron before the rearrangement (Figure 5), and after the rearrangement ($\Delta E = 1$ kcal/mol), they ligate to three oxygen atoms of two AlO_4^- tetrahedra and one oxygen atom of an SiO_4 tetrahedron.

Two closest six-rings across the LTA supercage can create two adjacent cationic sites. These rings face each other, but the sites are not parallel (Table 2). Two Fe–O_{Al} bonds and one Fe–O_{Si} bond are significantly shorter (1.96–2.06 Å) than the one Fe–O_{Al} bond (2.30 to 2.32 Å).

3.1.4. MOR _{β T1 β T1 and MOR _{β T3 β T3 Models.}} The optimized structures before and after the MD calculations are shown in Figures 6 and 7, respectively.

The MOR _{β T1 β T1 model greatly rearranges ($\Delta E = 11$ kcal/mol), while the MOR _{β T3 β T3 model only moderately changes ($\Delta E = 3$ kcal/mol) by the MD calculations. The Fe(II) cations in the former coordinate to two oxygen atoms of an AlO_4^- tetrahedron and two oxygen atoms of a SiO_4 tetrahedron before the MD calculations, while they ligate to two oxygen atoms of two AlO_4^- tetrahedra and one oxygen atom of an SiO_4 tetrahedron. Conversely, the latter features the proper^{21,29} coordination of Fe(II) to four oxygen atoms of two AlO_4^- tetrahedra before and after the MD calculations.}}

β Cationic sites in the mordenite structure are located at the bottom of the mordenite pocket. They are accessible only through eight-rings from the main channel. The mutual geometrical position of the two cationic sites and the Fe...Fe distance are shown in Table 2. The Fe–O_{Al} bonds are significantly shorter (2.04–2.07 Å) than the Fe–O_{Si} bonds (2.20–2.23 Å) in the MOR _{β T1 β T1 model, while all the Fe–O}

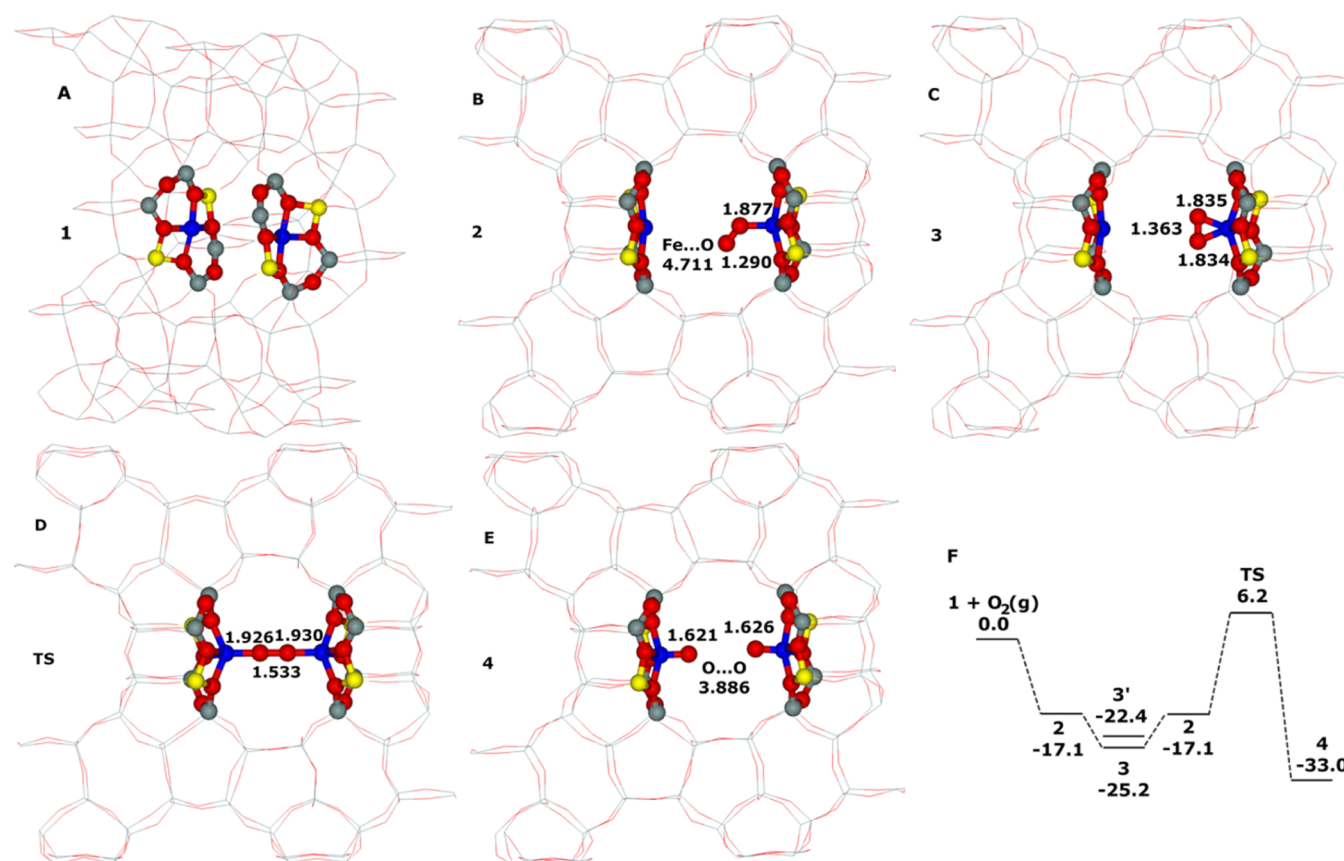


Figure 9. $BEA_{\beta T5\beta T6}$ model. Optimized structures for the (A) two opposite $\beta T5$ and $\beta T6$ sites of the Fe-beta zeolite 1 after molecular dynamics (MD) simulations, (B) monodentate $[Fe\ OO_{mono}\cdots Fe]$ complex 2, (C) bidentate $[Fe\ OO_{bi}\cdots Fe]$ complex 3, (D) $[Fe-O-O-Fe]$ transition state TS, and (E) $[Fe=O\ O=Fe]$ product 4. The distances are in Å. Silicon atoms are in gray, oxygen atoms are in red, aluminum atoms are in yellow, and iron atoms are in blue. Schematic energy profile (in kilocalorie per mol) for (F) the formation of the $Fe=O\ O=Fe$ product 4.

bond lengths of the $MOR_{\beta T3\beta T3}$ model are almost identical (2.13–2.19 Å).

3.2. Splitting Dioxygen. **3.2.1. $FER_{\beta 1\beta 1}$ Model.** Dioxygen, which is a triplet, adsorbs on one of the Fe(II) cations to yield a $[Fe\ OO_{mono}\cdots Fe]'$ monodentate complex $2'$ possessing the O_2 moiety in a triplet state. The calculated adsorption energy is -10.8 kcal/mol. $2'$ either undergoes a spin change to yield a $[Fe\ OO_{mono}\cdots Fe]$ monodentate complex 2 (the energy drops by 2.5 kcal/mol) which has the O_2 moiety in a singlet state or rearranges its structure to form a $[Fe\ OO_{bi}\cdots Fe]'$ bidentate complex $3'$ (the calculated adsorption energy is -16.9 kcal/mol). In the latter case, a spin crossover takes place and a $[Fe\ OO_{bi}\cdots Fe]$ bidentate complex 3 with the O_2 moiety in a singlet state is yielded. 3 is more stable than $3'$ by 4.0 kcal/mol. The bidentate complex 3 is more stable; however, the O_2 moiety of the less stable monodentate complex 2 is better positioned to interact with the other Fe(II) located in the adjacent $\beta 1$ site. Afterward, a cleavage of dioxygen occurs via a $[Fe-O-O-Fe]$ transition state TS to form a $[Fe=O\ O=Fe]$ complex 4 in a concerted manner. Both Fe in 4 are oxidized to form a pair of the α -oxygen atoms. The calculated reaction energy of the reaction from $1 + O_2(g)$ to give 4 is -23.3 kcal/mol (Table 2). The calculated barrier of the cleavage of dioxygen is 21.3 kcal/mol (Table 2), indicating that this system is calculated to be capable of splitting dioxygen. The optimized structures of 1, 2, 3, TS, and 4 and the energy profile of splitting dioxygen are shown in Figure 8.

Our calculations reveal that the $[Fe=O\ O=Fe]$ complex 4 with eight unpaired electrons really represents the ground state. The iterative Hirshfeld charges⁵⁴ are +1.75 for the Fe cation and -0.39 for the α -oxygen atom, revealing that the complex 4 corresponds mainly to the $[Fe(IV)=O\ O=Fe(IV)]^{4+}$ structure balanced by four Al atoms of the zeolite framework.

3.2.2. $BEA_{\beta T5\beta T6}$, $BEA_{\beta T7\beta T8}$, LTA, and $MOR_{\beta T1\beta T1}$ Models. Figures 9–12 show that the mechanism of the dioxygen cleavage to yield a pair of the α -oxygen atoms is the same as that for the $FER_{\beta 1\beta 1}$ model. The difference is that we could locate a $[Fe\ OO_{mono}\cdots Fe]'$ monodentate complex $2'$ for neither $BEA_{\beta T5\beta T6}$ nor $BEA_{\beta T7\beta T8}$. In addition, the bidentate $[Fe\ OO_{bi}\cdots Fe]'$ complex $3'$ with the O_2 moiety in a triplet state is more stable than 3 which has the O_2 moiety in a singlet state for $MOR_{\beta T1\beta T1}$. The calculated reaction energies (Table 2) of the reaction from $1 + O_2(g)$ to give 4 are -33.0 , -32.6 , -22.7 , and -19.2 kcal/mol for $BEA_{\beta T5\beta T6}$, $BEA_{\beta T7\beta T8}$, LTA, and $MOR_{\beta T1\beta T1}$, respectively. The calculated barriers (Table 2) of the cleavage of dioxygen are 31.4, 31.2, 61.6, and 15.0 kcal/mol, respectively, indicating that the beta zeolite and, especially, the mordenite with Fe(II) in two adjacent $\beta T1$ sites are calculated to be capable of splitting dioxygen, while the A zeolite is not. The optimized structures of 1, 2, 3, TS, and 4 and the energy profile of splitting dioxygen are shown in Figures 9–12 for the $BEA_{\beta T5\beta T6}$, $BEA_{\beta T7\beta T8}$, LTA, and $MOR_{\beta T1\beta T1}$ models, respectively.

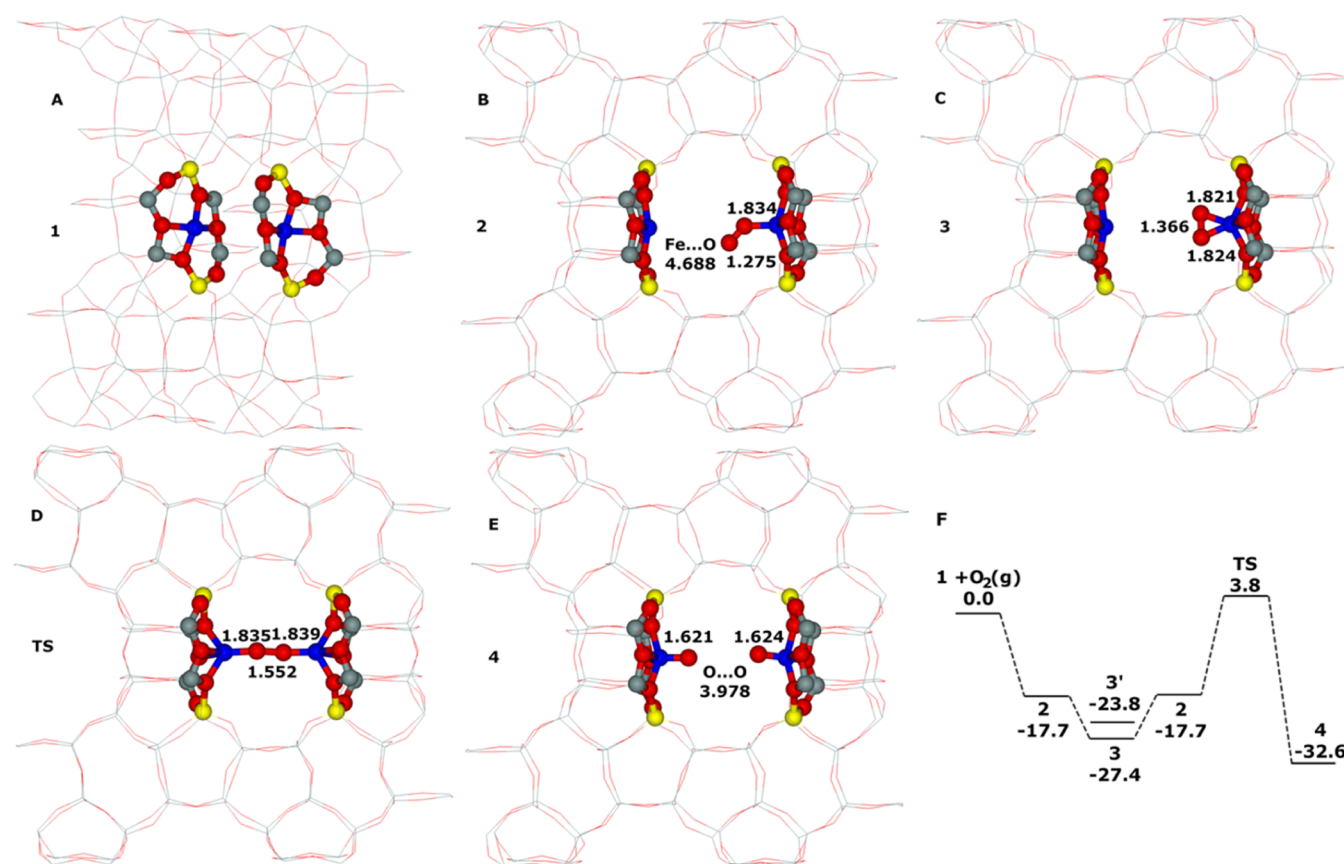


Figure 10. $\text{BEA}_{\beta T7\beta T8}$ model. Optimized structures for the (A) two opposite $\beta T7$ and $\beta T8$ sites of the Fe-beta zeolite **1** after molecular dynamics (MD) simulations, (B) monodentate $[\text{Fe OO}_{\text{mono}}\cdots\text{Fe}]$ complex **2**, (C) bidentate $[\text{Fe OO}_{\text{bi}}\cdots\text{Fe}]$ complex **3**, (D) $[\text{Fe}-\text{O}-\text{O}-\text{Fe}]$ transition state **TS**, and (E) $[\text{Fe}=\text{O O}=\text{Fe}]$ product **4**. The distances are in \AA . Silicon atoms are in gray, oxygen atoms are in red, aluminum atoms are in yellow, and iron atoms are in blue. Schematic energy profile (in kilocalorie per mol) for (F) the formation of the $\text{Fe}=\text{O O}=\text{Fe}$ product **4**.

3.2.3. $\text{FER}_{\alpha\alpha}$ and $\text{MOR}_{\beta T3\beta T3}$ Models. The results of our calculations for the $\text{FER}_{\alpha\alpha}$ (Figure 13A) and $\text{MOR}_{\beta T3\beta T3}$ models (Figure 13B) reveal that the cleavage of dioxygen cannot occur. We could locate a $[\text{Fe}-\text{O}-\text{O}-\text{Fe}]$ transition state **TS** for neither $\text{FER}_{\alpha\alpha}$ nor $\text{MOR}_{\beta T3\beta T3}$.

4. DISCUSSION

The results of our DFT calculations clearly show that (i) the local structure of the two cationic sites forming the distant binuclear Fe(II) sites and (ii) the mutual geometrical position of these two Fe(II) sites only roughly reflect the structure of the zeolite without the presence of divalent cations in the rings forming the cationic sites (hereafter the “empty” zeolite). The optimized structures of **1**, **2**, **3**, **TS**, and **4** and the energy profile of splitting dioxygen are shown in Figure 14 for the $\text{FER}_{\beta 2\beta 2}$ model of our prior study⁴ for better clarity and intelligibility of the discussion.

Binding the cation often causes a significant rearrangement of the site to get the optimal Fe–O distances and the ligation of Fe to four O atoms of two AlO_4^- tetrahedra if the structure of the zeolite allows. This is in sound agreement with the previous FTIR experiments coupled with periodic DFT calculations including MD simulations regarding the siting of divalent cations in ferrierite.²⁹ Nevertheless, although a significant rearrangement of the cationic site can occur, the mutual geometrical position of the cationic sites (i.e., facing or not facing each other, parallel or nonparallel, and if parallel, whether axial or nonaxial) related to the structure of the

“empty” zeolite is preserved if the cationic site is formed by a six-ring. Conversely, the rearrangement of an eight-ring caused by cation binding can induce such a rearrangement of the local structure that the mutual geometrical position of the cationic sites changes relative to the “empty” zeolite. Such a rearrangement can be hardly suggested based only on the structure of the “empty” zeolite. Moreover, even for six-rings forming cationic sites, the final arrangement of the distant binuclear Fe(II) sites can be far from those based only on empty six-rings. Although the mutual geometrical position of the cationic sites is preserved, the Fe \cdots Fe distance can be significantly shortened compared to the distance of the empty six-rings for some zeolites (Table 2). For example, the distance between the planes of the two 6-rings at the opposite sides of the wall of the 12-ring channel of the beta zeolite is ca. 9.5 \AA , while the calculated Fe \cdots Fe distances are significantly shorter (7.63 and 7.61 \AA for the $\text{BEA}_{\beta T5\beta T6}$ and $\text{BEA}_{\beta T7\beta T8}$ models, respectively). The distance between the two empty rings represents only the largest possible distance of the cations. The Fe \cdots Fe distance cannot be derived from results of diffraction experiments but can be inferred from periodic DFT calculations including MD simulations (or other global optimizations), allowing a possible rearrangement of the cationic sites. Moreover, this theoretical treatment is also required to determine the mutual geometrical position of the two cationic sites created by two eight-rings as this cannot be obtained from results of diffraction experiments either.

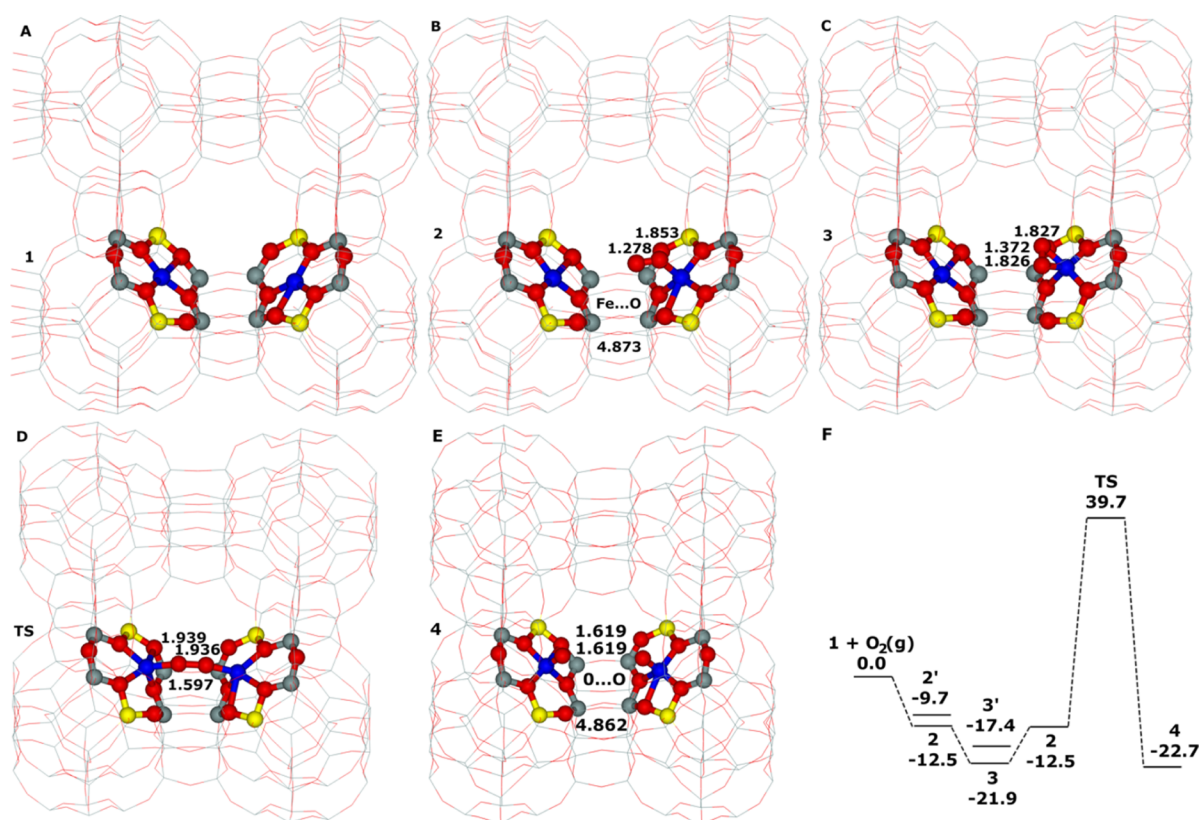


Figure 11. LTA model. Optimized structures for the (A) two adjacent six-ring sites of the Fe-A zeolite 1 after molecular dynamics (MD) simulations, (B) monodentate [Fe OO_{mono}...Fe] complex 2, (C) bidentate [Fe OO_{bi}...Fe] complex 3, (D) [Fe–O–O–Fe] transition state TS, and (E) [Fe=O O=Fe] product 4. The distances are in Å. Silicon atoms are in gray, oxygen atoms are in red, aluminum atoms are in yellow, and iron atoms are in blue. Schematic energy profile (in kilocalorie per mol) for (F) the formation of the Fe=O O=Fe product 4.

The results obtained clearly indicate that the capability of splitting dioxygen at room temperature is not unique to Fe-ferrierite⁴ but the distant binuclear Fe(II) centers able to cleave dioxygen can be, in general, prepared in zeolite matrices with various topologies (note that procedures to obtain the Al distribution required for the preparation of these sites are not discussed here). However, splitting dioxygen can occur only for some arrangements of the two Fe(II) sites. The distance between two Fe cations is without any doubt one of the key parameters controlling the activity of the centers in splitting dioxygen. Because several distant binuclear Fe(II) centers formed in various zeolites differ in the Fe...Fe distance while the two sites face each other and are parallel and axial, the effect of the Fe...Fe distance is discussed first. The distances between the two Fe cations in the distant binuclear sites and the corresponding energy barriers for splitting dioxygen are listed in Table 2. It is clear that for some zeolites, the distance between the two cations can be significantly shortened compared to the distance of the empty rings. This can be explained by the fact that the optimum Fe(II)–O_{FR} distances and the preferential binding of Fe(II) to oxygen atoms of two AlO₄⁻ tetrahedra can be reached only when the cation is located above the ring plane. If the Fe...Fe distance is too short (5.64 Å for the FER_{aa} model; Figure 1 and Table 2), then the μ -peroxo diiron species (Figure 13A) is formed and the cleavage of dioxygen cannot occur. This arrangement (Figure 13A) might resemble the oxidized form of the active site of the methane monooxygenase and the CuO₂Cu bridging species suggested as the active site for direct oxidation of methane over Cu-zeolites.^{5,8,13} Although the activity of such μ -peroxo diiron

species in the oxidation reaction cannot be excluded, an investigation of this type of dioxygen activation is out of the scope of this study.

The calculated barriers are plotted against the Fe...Fe distances in Figure 15. We can estimate, based on this plot and Table 2, that there is an optimum distance of around 7–7.3 Å between the two Fe(II) cations corresponding to the lowest barrier for splitting dioxygen. The Fe...Fe distance of 7.261 Å calculated for the mordenite zeolite with two adjacent β T1 cationic sites (MOR _{β T1/ β T1}) is most likely close to the ideal Fe...Fe distance for splitting dioxygen as the calculated barrier of 15.0 kcal/mol (Table 2) is very low. On the one hand, if the Fe...Fe distance is significantly smaller than ca. 7 Å, then an oxo-bridge species can form and splitting cannot occur. On the other hand, if the Fe...Fe distance is markedly larger than ca. 8 Å, then the zeolite is incapable of splitting dioxygen as well since the corresponding transition state TS cannot form.

Not only the Fe...Fe distance but also the mutual geometrical position of the cationic sites (i.e., facing or not facing each other, parallel or nonparallel, and if parallel, whether axial or nonaxial) are crucial for splitting dioxygen to occur with a low barrier. As calculated for the FER _{β 1/ β 1}, FER _{β 2/ β 2}, BEA _{β T5/ β T6}, BEA _{β T7/ β T8}, and MOR _{β T1/ β T1} models, the transition states of the cleavage of dioxygen are approximately linear. The crucial role of the linear arrangement, given by the position of the two Fe cations, is illustrated by the Fe-A zeolite (the LTA model). Although an Fe...Fe distance of 7.33 Å (Table 2) fits well into the region of a low barrier for splitting dioxygen (Figure 15), the calculated barrier of 62 kcal/mol (Table 2) is more than twice higher. The nonparallel mutual

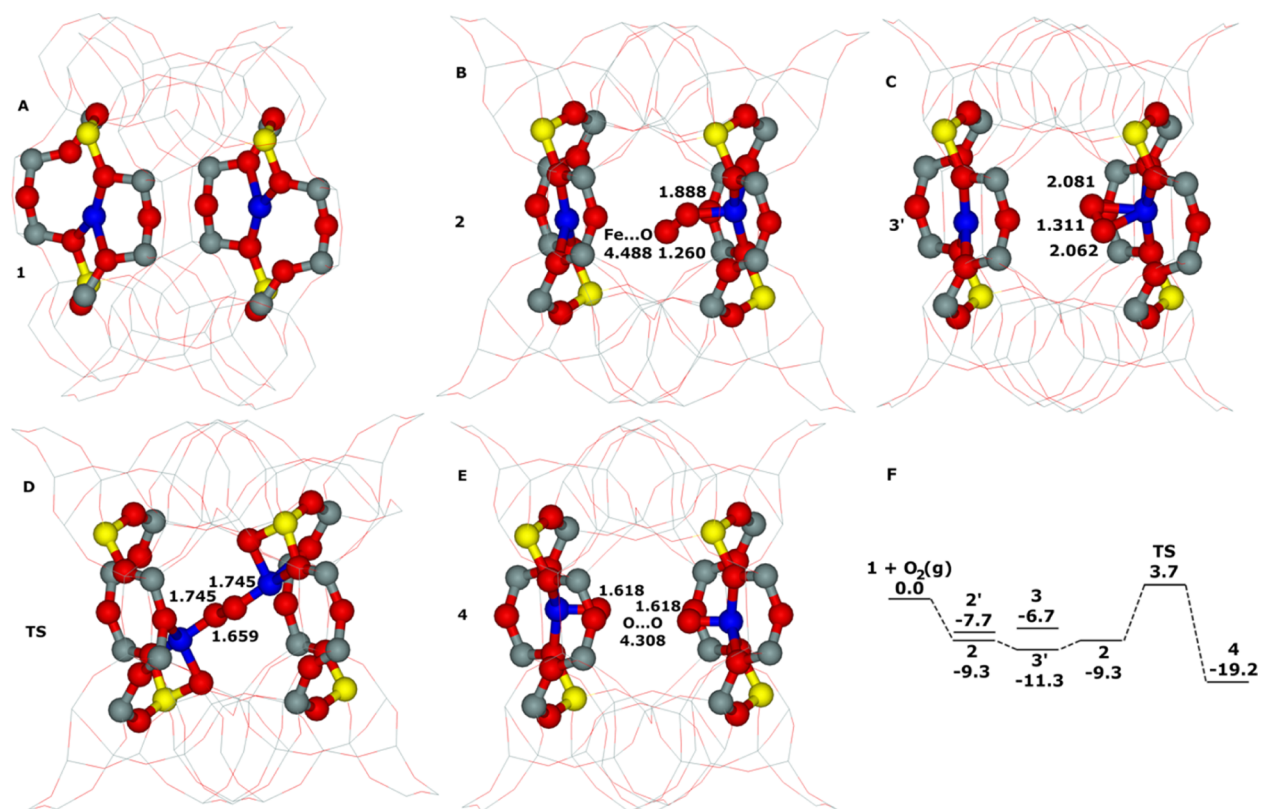


Figure 12. MOR _{β T1/ β T1} model. Optimized structures for the (A) two adjacent β T1 sites of Fe-mordenite 1 after molecular dynamics (MD) simulations, (B) monodentate [Fe OO_{mono}...Fe] complex 2, (C) bidentate [Fe OO_{bi}...Fe] complex 3', (D) [Fe–O–O–Fe] transition state TS, and (E) [Fe=O O=Fe] product 4. The distances are in Å. Silicon atoms are in gray, oxygen atoms are in red, aluminum atoms are in yellow, and iron atoms are in blue. Schematic energy profile (in kilocalorie per mol) for (F) the formation of the Fe=O O=Fe product 4.

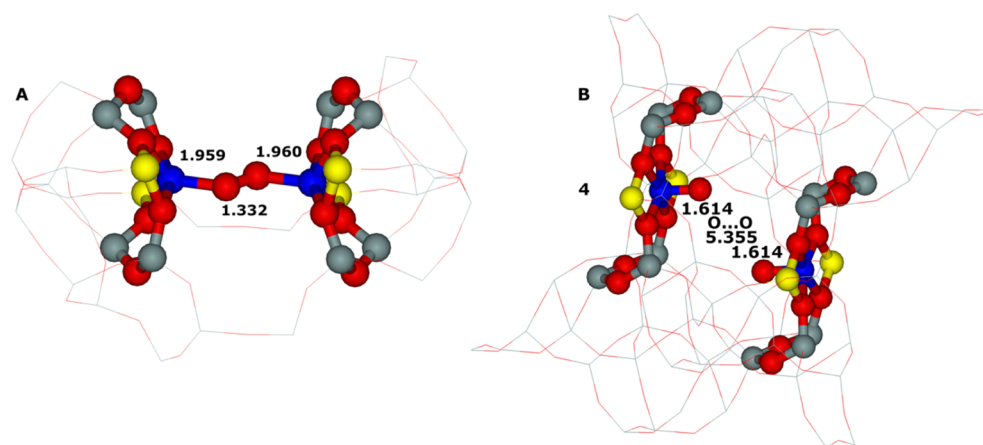


Figure 13. Optimized structures for the (A) μ -peroxo diiron (FER _{α} model) structure and (B) [Fe=O O=Fe] (MOR _{β T3/ β T3} model) product 4. The distances are in Å. Silicon atoms are in gray, oxygen atoms are in red, aluminum atoms are in yellow, and iron atoms are in blue.

geometrical position results in a nonlinear transition state and makes the Fe-A zeolite incapable of splitting dioxygen. Similarly, while the two adjacent β T3 sites of mordenite are parallel, they do not have a common axis. This mutual arrangement prohibits splitting dioxygen to occur despite the fact that a Fe...Fe distance of 7.55 Å (Table 2) still lies in the range of lower barriers (Figure 15).

The Al siting in the rings forming the cationic sites is another parameter which can affect the arrangement of the cations in their sites and thus splitting dioxygen as well. The reason is that various Al sitings in the rings can result in

different rearrangements of the cationic site upon binding the divalent cation.

Divalent cations are charge-balanced by two Al atoms located in the ring forming the corresponding cationic site. Periodic DFT calculations including molecular dynamics showed that divalent cations preferred the proper coordination to four oxygen atoms of two AlO₄⁻ tetrahedra.^{21,28–30} The proper binding of the divalent cation can lead to a significant rearrangement of the cationic site and, therefore, also to a marked change in the local structure of the cationic site. The rearrangement of the cationic sites is reflected in the

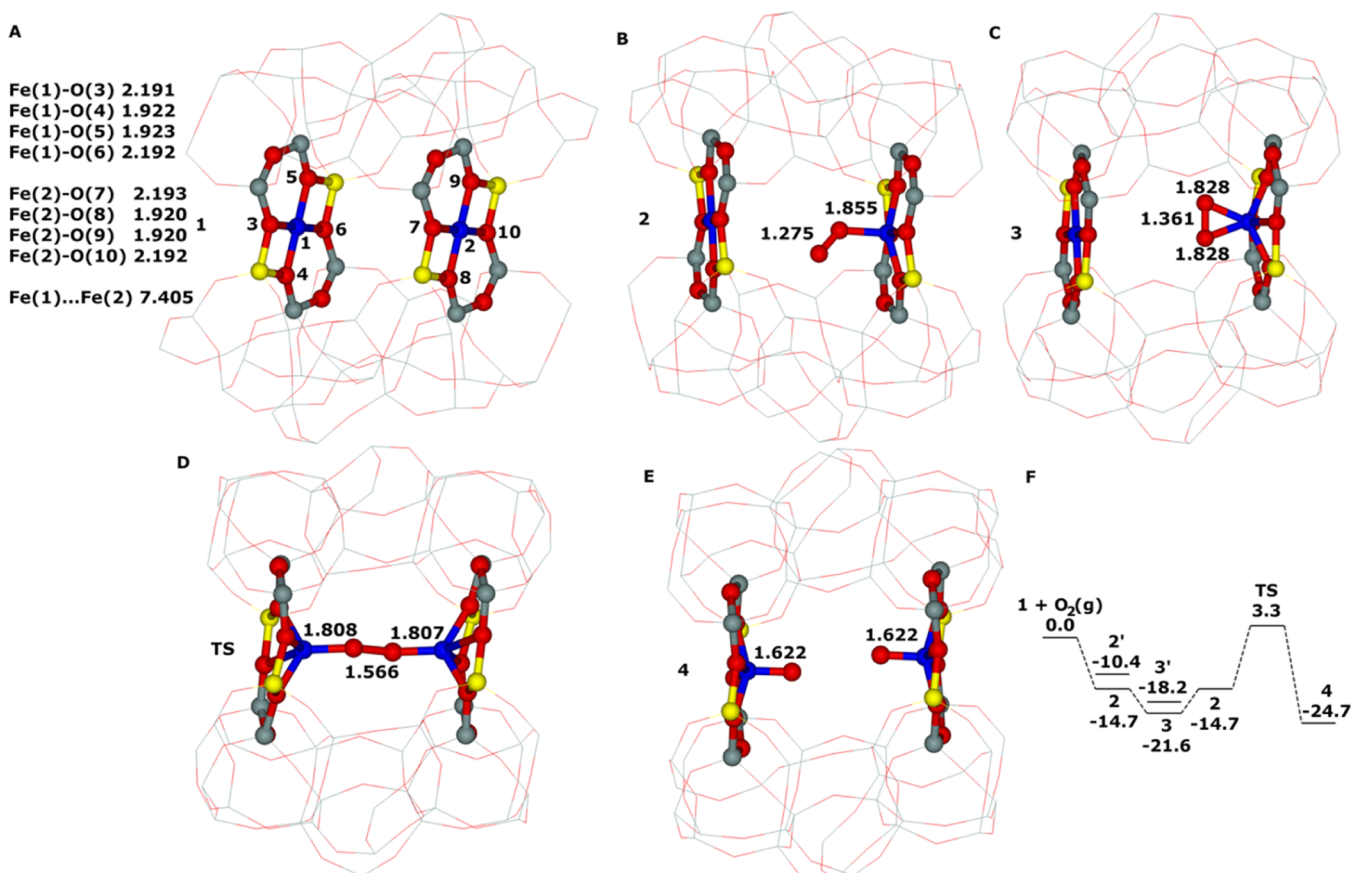


Figure 14. FER $_{\beta_2\beta_2}$ model. Optimized structures for the (A) two adjacent β_2 sites of Fe-ferrierite **1** after molecular dynamics (MD) simulations, (B) monodentate [Fe OO $_{\text{mono}}$...Fe] complex **2**, (C) bidentate [Fe OO $_{\text{bi}}$...Fe] complex **3**, (D) [Fe–O–O–Fe] transition state TS, and (E) [Fe=O O=Fe] product **4**. The distances are in Å. Silicon atoms are in gray, oxygen atoms are in red, aluminum atoms are in yellow, and iron atoms are in blue. Schematic energy profile (in kilocalorie per mol) for (F) the formation of the Fe=O O=Fe product **4**. Adapted Figure 1 from ref 4 licensed under a Creative Commons Attribution License 4.0 (CC BY). <https://creativecommons.org/licenses/by/4.0/>.

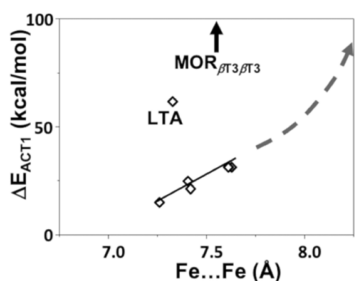


Figure 15. Barrier ΔE_{ACT1} plotted against the Fe...Fe distance for the FER $_{\beta_1\beta_1}$, FER $_{\beta_2\beta_2}$, BEA $_{\beta_5\beta_6}$, BEA $_{\beta_7\beta_8}$, LTA, MOR $_{\beta_1\beta_1}$, and MOR $_{\beta_3\beta_3}$ models.

stabilization energies (Table 1). The stabilization energy is the difference between the additional binding energy of the divalent cation due to the preferential binding to oxygen atoms of two AlO_4^- tetrahedra and the energy needed to deform the structure of the zeolite framework to permit the preferential binding of the divalent cation. The proper coordination of the divalent cation to four oxygen atoms of two AlO_4^- tetrahedra can be reached only for the cationic sites for which the additional binding energy is larger than the energy needed to deform the structure (i.e., FER $_{\text{aw}}$, FER $_{\beta_1\beta_1}$, FER $_{\beta_2\beta_2}$, BEA $_{\beta_5\beta_6}$, and MOR $_{\beta_3\beta_3}$).^{21,28–30,35} The rearrangement of cationic sites upon binding divalent cations was confirmed by FTIR spectroscopy for ferrierite.²⁹

The rearrangement of cationic sites is calculated only for the structure **1** featuring two Fe(II) cations for each computational model. The subsequent calculations of the complexes **2** and **3**, the transition state TS, and the product **4** for each computational model use the corresponding previously rearranged structure **1** as the starting geometry already featuring the preferential binding of Fe(II) to oxygen atoms of two AlO_4^- tetrahedra.

In addition, the rearrangement of the cationic sites can also cause a change in the mutual geometrical position (i.e., facing or not facing each other, parallel or nonparallel, and if parallel, whether axial or nonaxial) and the Fe...Fe distance of the cationic sites forming the distant binuclear sites.

Our results (Figures 1–7 and Table 2) clearly show that the variability of the Al siting can result in the rearrangement of the cationic site for both six-rings and eight-rings but the effect of the Al siting on the cleavage of dioxygen is negligible for six-rings, while is decisive for eight-rings. The explanation of the different influence of the Al siting on six-rings and eight-rings is the conservation of the mutual geometrical position (including the Fe...Fe distance) of the cationic sites formed by six-rings after their rearrangement with respect to the structure of the “empty” zeolite. The plane of the rearranged cationic site formed by a six-ring is identical/close to that of the same six-ring of the “empty” zeolite. This does not have to hold for cationic sites formed by eight-rings. The latter are formed by eight oxygen atoms, and when a divalent cation binds, it is

coordinated to only three (Figure 6) or four (Figure 7) oxygen atoms. Accordingly, the formed cationic sites can possess different planes depending on the Al siting in that eight-ring (Figures 6 and 7). Consequently, the mutual geometrical position of the cationic sites created by eight-rings can change relative to the “empty” zeolite upon binding divalent cations. Therefore, we can conclude that since the mutual geometrical position and the Fe...Fe distance of the two Fe(II) cations creating the distant binuclear Fe species are the same for all the Al sitings in the six-ring forming the corresponding cationic site of the same zeolite (i.e., $\beta 1$ and $\beta 2$ of ferrierite and $\beta T5/\beta T6$ and $\beta T7/\beta T8$ of the beta zeolite), the capability of splitting dioxygen is identical, regardless of the Al siting in that six-ring (Table 2). Conversely, since the mutual geometrical position and the Fe...Fe distance of the two Fe(II) cations differ for various Al sitings in eight-rings, the ability to cleave dioxygen differs as well (Table 2).

The individual computational models are discussed in detail in the subsequent paragraphs 4.1 and 4.2.

4.1. FER $_{\beta 1\beta 1}$, FER $_{\beta 2\beta 2}$, BEA $_{\beta T5\beta T6}$, BEA $_{\beta T7\beta T8}$, and MOR $_{\beta T1\beta T1}$ Models Permitting the Formation of a Pair of the α -oxygen Atoms. The two cationic sites of the FER $_{\beta 1\beta 1}$ (Figure 2), FER $_{\beta 2\beta 2}$ (Figure 14), BEA $_{\beta T5\beta T6}$ (Figure 3), BEA $_{\beta T7\beta T8}$ (Figure 4), and MOR $_{\beta T1\beta T1}$ (Figure 6) models face each other and are parallel and axial. The distances of the two Fe(II) cations lie in a narrow range (Table 2). The smallest Fe...Fe distance of 7.26 Å of MOR $_{\beta T1\beta T1}$ corresponds to the lowest barrier of 15.0 kcal/mol, while the largest Fe...Fe distance of 7.63 Å relates to the highest barrier of 31.4 kcal/mol (Table 2 and Figure 15). Our periodic DFT calculations reveal that the structure of the mordenite zeolite with two adjacent $\beta T1$ cationic sites (MOR $_{\beta T1\beta T1}$) is most likely close to the ideal structure for splitting dioxygen as the calculated barrier of 15.0 kcal/mol (Table 2) is very low.

4.2. FER $_{\alpha\alpha}$, LTA, and MOR $_{\beta T3\beta T3}$ Models Prohibiting the Creation of a Pair of the α -oxygen Atoms. The distance between two Fe(II) cations is calculated to be 5.64 Å in FER $_{\alpha\alpha}$ (Figure 1 and Table 2). The two cations are too close to each other to allow the formation of a pair of the α -oxygen atoms. Instead, a μ -peroxo diiron structure is created (Figure 13A).

The two Fe(II) cations in LTA are 7.33 Å from each other (Figure 5 and Table 2). The two rings forming the adjacent cationic sites face each other, but they are not parallel, causing a larger distance of 4.86 Å of the two α -oxygen atoms in the [Fe=O O=Fe] product 4 (Figure 11E). This value is the second largest among all the models used. Therefore, because of the nonparallel adjacent cationic sites, the geometry of the [Fe–O–O–Fe] transition state TS differs from those of the other calculated transition states, and the corresponding barrier is calculated to be 61.6 kcal/mol (Table 2). This value is very high showing that the A zeolite with Fe(II) in two closest six-rings across the LTA supercage is calculated to be incapable of splitting dioxygen. This result clearly shows the crucial importance of the requirement for the two sites forming the distant binuclear species to be parallel.

The two Fe(II) cations in MOR $_{\beta T3\beta T3}$ are 7.55 Å apart (Figure 7 and Table 2); however, while the two adjacent $\beta T3$ sites face each other and are parallel, they do not have a common axis. The distance of the two α -oxygen atoms is calculated to be 5.36 Å in the [Fe=O O=Fe] product 4 (Figure 13B). This value is the largest among all the models used and prohibits the occurrence of splitting dioxygen over

mordenite with the distant binuclear Fe(II) species stabilized in two adjacent $\beta T3$ sites. The large O...O distance is consistent with the fact that we could locate no [Fe–O–O–Fe] transition state TS for MOR $_{\beta T3\beta T3}$.

4.3. Effect of the Al Siting in the Rings Forming the Cationic Sites. Comparison of Figure 8F (FER $_{\beta 1\beta 1}$) and Figure 14F (FER $_{\beta 2\beta 2}$) reveals that the effect of the Al siting in the rings forming the cationic sites is essentially negligible, only the barrier is somewhat higher for FER $_{\beta 2\beta 2}$. Similarly, comparison of Figures 9F (BEA $_{\beta T5\beta T6}$) and 10F (BEA $_{\beta T7\beta T8}$) shows a negligible influence of the Al siting in the rings creating the cationic sites as well. Conversely, Figure 12F (MOR $_{\beta T1\beta T1}$) reveals that the mordenite with Fe(II) in two adjacent $\beta T1$ sites is calculated to be capable of splitting dioxygen, while Figure 13B (MOR $_{\beta T3\beta T3}$) shows that the same zeolite with Fe(II) in two adjacent $\beta T3$ sites is not. We can safely conclude that the Al siting in the rings creating the cationic sites has a negligible effect on splitting dioxygen if the local structures of the cationic sites are very similar and their mutual geometrical positions are the same for a particular zeolite (i.e., $\beta 1$ and $\beta 2$ of ferrierite and $\beta T5/\beta T6$ and $\beta T7/\beta T8$ of the beta zeolite). However, if the structures and the mutual geometrical positions of the cationic sites with various Al sitings in the rings creating these centers for a particular zeolite significantly differ, then the effect on splitting dioxygen can be huge. Therefore, the influence of the Al siting in the rings forming the cationic sites on the cleavage of dioxygen is only indirect through the change in the local structure of the active centers and their mutual geometrical positions.

4.4. Structural Parameters Allowing Splitting Dioxygen over the Distant Binuclear Fe(II) Species. The results of our periodic DFT calculations reveal that the activity regarding splitting dioxygen represents a general property of the distant binuclear Fe(II) centers stabilized in the aluminosilicate matrix if four conditions are fulfilled. The two cationic sites forming the distant binuclear Fe(II) centers have to (i) face each other, (ii) be parallel, and (iii) be axial. (iv) The Fe...Fe distance has to lie in a narrow range from ca. 7 to ca. 8 Å.

The activity in splitting dioxygen, which is determined predominantly by the barrier of this reaction, is essential for the development of the zeolite systems with the distant binuclear Fe(II) centers as catalysts for the direct oxidation of methane. Nevertheless, the recombination of dioxygen has to be taken in the account as well. The corresponding energy barrier is included in Table 2. The reverse barrier ΔE_{ACT2} correlates well with the barrier ΔE_{ACT1} of splitting dioxygen (Table 2) because both the processes depend on the Fe...Fe distance. The ΔE_{ACT2} values are larger than the ΔE_{ACT1} ones by 1 (LTA)–8 (MOR $_{\beta T1\beta T1}$) kcal/mol (i.e., the $\Delta\Delta E_{ACT}$ values in Table 2). The $\Delta\Delta E_{ACT}$ values also correspond to the difference in stability of the product 4 and the bidentate complex 3 (3' for MOR $_{\beta T1\beta T1}$). 4 is more stable than the bidentate complex 3 (3' for MOR $_{\beta T1\beta T1}$) for all the computational models (Table 2), indicating that the equilibrium is shifted toward the product 4. For the computational models of interest (i.e., excluding the LTA model owing to the huge barrier and the FER $_{\beta 1\beta 1}$ model because of the absence of ferrierite with the corresponding Al siting), 4 is more stable than 3 by 3 (FER $_{\beta 2\beta 2}$)–10 (MOR $_{\beta T1\beta T1}$) kcal/mol establishing, essentially, the exclusive presence of 4 in the zeolite after the oxidation of the Fe(II) cations by dioxygen.

The results discussed above show that the capability of splitting dioxygen is general for the distant binuclear Fe(II) sites. Although the Fe...Fe distance is crucial for the ability of the zeolite to split dioxygen, the proper mutual geometrical position (i.e., facing or not facing each other, parallel or nonparallel, and if parallel, whether axial or nonaxial) of the two cationic sites forming the distant binuclear sites is also essential to allow the formation of an approximately linear transition state TS which is a key to the occurrence of the cleavage of dioxygen. Our calculations reveal that both these required parameters could be reached in other zeolite topologies and thus suggest the possibility of developing Fe-zeolite-based systems for the dioxygen activation employed for direct oxidations using other zeolite matrices. From the topological point of view, there are a number of possible zeolite candidates which are able to form distant binuclear Fe(II) sites active in splitting dioxygen. Nevertheless, the accommodation of two cooperating Fe(II) cations forming distant binuclear sites requires a specific organization of Al atoms in the framework. The two adjacent/opposite zeolite rings have to contain two framework Al atoms each (i.e., four Al atoms in total). This requires both a high relative concentration of Al atoms in the form of Al pairs and a high total concentration of Al atoms in the framework. To the best of our knowledge, the number of such Si-rich zeolite matrices is limited at the present time. Therefore, the development of new materials possessing the capability of splitting dioxygen will require syntheses of zeolite matrices with the desired Al organizations. Because the preparation of zeolites with the desired concentration and siting of the Al pairs forming the cationic sites is difficult and very time-demanding, suitable DFT calculations are an essential part of the development of Fe-zeolite systems for splitting dioxygen and subsequent applications. Nevertheless, a preliminary selection of appropriate zeolite structural types can be made based on the analysis of the topology of the zeolite framework. Promising zeolite materials should meet the criteria as follows: they can be prepared with (i) high enough concentrations of Al atoms in the framework ($\text{Si}/\text{Al} < \text{ca. } 10$ depending on the topology), (ii) high enough concentrations of Al pairs, allowing a significant presence of two adjacent/opposite rings with two Al pairs (this has to be estimated individually for each specific topology), for details see our prior studies,^{4,21,22} and (iii) two six-rings facing each other, being parallel and axial with the distance between the two rings in empty zeolites in the range from ca. 7 to ca. 10 Å. It should be noted that the corresponding Fe...Fe distance can be significantly shorter compared to that of the empty rings. Nevertheless, the maximum distance is not strictly given. Moreover, eight-rings can form the distant binuclear sites with the axial arrangements as well. Following these criteria represents the starting point in the process of the development of highly active catalysts for direct oxidation reactions using dioxygen (including that of methane to methanol) and, moreover, with the possibility of tuning their properties for individual oxidation reactions. It should be noted that the application of dioxygen as the oxidant is highly desirable due to the economic, safety (compare with H_2O_2), and environmental (compare with N_2O) reasons. The utilization of O_2 as the oxidant can be regarded as a key factor for the development of new technologies fulfilling the requirements on green and sustainable chemical production. Nevertheless, in the case of bulkier molecules than methane, the accessibility of the active oxygen species by these

molecules, that is, the location of the distant binuclear Fe(II) sites in the zeolite channel system (eight-, ten-, or twelve-ring channel), should be decisive. We can safely conclude that the selection of suitable zeolite structures is only the first, and probably simplest, step in this process which has to be followed by a preparation of zeolite matrices with the Al content and the Al organization, allowing the formation of the adequate concentrations of the distant binuclear cationic Fe(II) centers.

5. CONCLUSIONS

The distant binuclear cationic Fe(II) centers in Fe-zeolite of the ferrierite topology were shown to split dioxygen at room temperature and directly oxidize methane to methanol at room temperature as well. Theoretical modeling clearly shows that this breakthrough in the activation of dioxygen is not limited exclusively to matrices of the ferrierite topology. Periodic DFT calculations including MD simulations of the distant binuclear Fe(II) centers accommodated in the ferrierite, beta, A, and mordenite zeolites with various Al sitings in the rings forming the cationic sites were employed to study the effects of (i) the Al siting in the rings forming the cationic sites, (ii) the distance, and (iii) the mutual geometrical position of the rings accommodating Fe(II) on the activity of the distant binuclear Fe(II) sites in splitting dioxygen.

Our results reveal that the distant binuclear Fe(II) sites with suitable parameters accommodated in various zeolites can split dioxygen and form a pair of oxygen species called the α -oxygen, which were reported to be very active in the oxidation of methane to methanol. Therefore, the ability to cleave dioxygen represents a general property of the distant binuclear Fe(II) centers stabilized in aluminosilicate matrices, thus suggesting the possibility of developing Fe-zeolite-based systems for the dioxygen activation for direct oxidations using various zeolite matrices. The suitable parameters are found to be the two cationic sites forming the distant binuclear Fe(II) centers have to (i) face each other, (ii) be parallel, and (iii) be axial. (iv) The Fe...Fe distance has to lie in a narrow range from ca. 7 to ca. 8 Å (ca. 7–ca. 10 Å for the distance between the two rings (forming the corresponding cationic sites) in empty zeolites since this distance is equal or larger than the Fe...Fe distances). The α -oxygen atoms formed by splitting dioxygen over the distant binuclear Fe(II) sites were reported to be highly active in the oxidation of methane to methanol even at room temperature, and moreover, methanol was released from the active sites with no need of an effluent in contrast to the other systems. Thus, the capability of various zeolite structures, allowing a formation of the distant binuclear Fe(II) sites active in the activation of dioxygen, opens the possibility of developing highly active and selective systems employed for the direct oxidation of (i) methane to methanol and (ii) other organic compounds to valuable oxidation products. Such systems will have tunable properties, that is, (i) the transport properties, (ii) the accessibilities of the active α -oxygen atoms, (iii) the barriers of the cleavage of dioxygen and the recombination of dioxygen, and (iv) the reactivities of the corresponding α -oxygen atoms in oxidation reactions. Nevertheless, the candidate zeolite materials for the direct oxidation by the α -oxygen atoms formed by splitting dioxygen should also fulfill other requirements. They have to be preparable with high enough concentrations of Al atoms in the framework ($\text{Si}/\text{Al} < \text{ca. } 10$ depending on the topology), and moreover, a large part of the framework Al should correspond to Al pairs,

allowing a significant presence of two adjacent/opposite rings with two Al pairs able to accommodate two Fe(II) cations.

AUTHOR INFORMATION

Corresponding Author

Stepan Sklenak – J. Heyrovský Institute of Physical Chemistry, The Czech Academy of Sciences, 18223 Prague, Czech Republic; orcid.org/0000-0003-4862-857X; Email: stepan.sklenak@jh-inst.cas.cz

Authors

Edyta Tabor – J. Heyrovský Institute of Physical Chemistry, The Czech Academy of Sciences, 18223 Prague, Czech Republic; orcid.org/0000-0002-4071-8610

Mariia Lemishka – J. Heyrovský Institute of Physical Chemistry, The Czech Academy of Sciences, 18223 Prague, Czech Republic; Department of Physical Chemistry, Faculty of Chemical Technology, University of Pardubice, 530 10 Pardubice, Czech Republic

Joanna E. Olszowska – J. Heyrovský Institute of Physical Chemistry, The Czech Academy of Sciences, 18223 Prague, Czech Republic

Kinga Mlekodaj – J. Heyrovský Institute of Physical Chemistry, The Czech Academy of Sciences, 18223 Prague, Czech Republic; orcid.org/0000-0003-3242-6535

Jiri Dedecek – J. Heyrovský Institute of Physical Chemistry, The Czech Academy of Sciences, 18223 Prague, Czech Republic

Prokopis C. Andrikopoulos – J. Heyrovský Institute of Physical Chemistry, The Czech Academy of Sciences, 18223 Prague, Czech Republic

Complete contact information is available at: <https://pubs.acs.org/10.1021/acscatal.0c04459>

Notes

The authors declare no competing financial interest.

ACKNOWLEDGMENTS

This work was supported by the Czech Science Foundation under projects # 17-00742S and the RVO: 61388955 and by Czech Academy of Sciences (Strategy AV21—Program Molecules and Materials for Life). This work was supported by The Ministry of Education, Youth and Sports from the Large Infrastructures for Research, Experimental Development and Innovations project “e-Infrastructure CZ—LM2018140”.

REFERENCES

(1) Snyder, B. E. R.; Vanelderen, P.; Bols, M. L.; Hallaert, S. D.; Böttger, L. H.; Ungur, L.; Pierloot, K.; Schoonheydt, R. A.; Sels, B. F.; Solomon, E. I. The active site of low-temperature methane hydroxylation in iron-containing zeolites. *Nature* **2016**, *536*, 317–321.

(2) Narsimhan, K.; Iyoki, K.; Dinh, K.; Román-Leshkov, Y. Catalytic oxidation of methane into methanol over copper-exchanged zeolites with oxygen at low temperature. *ACS Cent. Sci.* **2016**, *2*, 424–429.

(3) Dinh, K. T.; Sullivan, M. M.; Serna, P.; Meyer, R. J.; Dincă, M.; Román-Leshkov, Y. Viewpoint on the partial oxidation of methane to methanol using Cu- and Fe-exchanged zeolites. *ACS Catal.* **2018**, *8*, 8306–8313.

(4) Tabor, E.; Dedecek, J.; Mlekodaj, K.; Sobalik, Z.; Andrikopoulos, P. C.; Sklenak, S. Dioxxygen dissociation over man-made system at room temperature to form the active alpha-oxygen for methane oxidation. *Sci. Adv.* **2020**, *6*, eaaz9776.

(5) Snyder, B. E. R.; Bols, M. L.; Schoonheydt, R. A.; Sels, B. F.; Solomon, E. I. Iron and copper active sites in zeolites and their correlation to metalloenzymes. *Chem. Rev.* **2018**, *118*, 2718–2768.

(6) Lee, J. H.; Bonte, W.; Corthals, S.; Krumeich, F.; Ruitenbeek, M.; van Bokhoven, J. A. Zeolite nanoreactor for investigating sintering effects of cobalt-catalyzed Fischer-Tropsch synthesis. *Ind. Eng. Chem. Res.* **2019**, *58*, 5140–5145.

(7) Alayon, E. M.; Nachtegaal, M.; Ranocchiaro, M.; van Bokhoven, J. A. Catalytic conversion of methane to methanol over Cu-mordenite. *Chem. Commun.* **2012**, *48*, 404–406.

(8) Tao, L.; Lee, I.; Sanchez-Sanchez, M. Cu oxo nanoclusters for direct oxidation of methane to methanol: formation, structure and catalytic performance. *Catal. Sci. Technol.* **2020**, *10*, 7124–7141.

(9) Knorpp, A. J.; Pinar, A. B.; Newton, M. A.; Sushkevich, V. L.; van Bokhoven, J. A. Copper-exchanged omega (MAZ) zeolite: Copper-concentration dependent active sites and its unprecedented methane to methanol conversion. *ChemCatChem* **2018**, *10*, 5593–5596.

(10) Knorpp, A. J.; Newton, M. A.; Mizuno, S. C. M.; Zhu, J.; Mebrate, H.; Pinar, A. B.; van Bokhoven, J. A. Comparative performance of Cu-zeolites in the isothermal conversion of methane to methanol. *Chem. Commun.* **2019**, *55*, 11794–11797.

(11) Sushkevich, V. L.; Verel, R.; Bokhoven, J. A. Pathways of methane transformation over copper-exchanged mordenite as revealed by in situ NMR and IR spectroscopy. *Angew. Chem., Int. Ed.* **2020**, *59*, 910–918.

(12) Sushkevich, V. L.; van Bokhoven, J. A. Kinetic study and effect of water on methane oxidation to methanol over copper-exchanged mordenite. *Catal. Sci. Technol.* **2020**, *10*, 382–390.

(13) Newton, M. A.; Knorpp, A. J.; Sushkevich, V. L.; Palagin, D.; van Bokhoven, J. A. Active sites and mechanisms in the direct conversion of methane to methanol using Cu in zeolitic hosts: A critical examination. *Chem. Soc. Rev.* **2020**, *49*, 1449–1486.

(14) Ipek, B.; Lobo, R. F. Catalytic conversion of methane to methanol on Cu-SSZ-13 using N₂O as oxidant. *Chem. Commun.* **2016**, *52*, 13401–13404.

(15) Jovanovic, Z. R.; Lange, J.-P.; Ravi, M.; Knorpp, A. J.; Sushkevich, V. L.; Newton, M. A.; Palagin, D.; van Bokhoven, J. A. Oxidation of methane to methanol over Cu-exchanged zeolites: Scientia gratia scientiae or paradigm shift in natural gas valorization? *J. Catal.* **2020**, *385*, 238–245.

(16) Panov, G. I.; Sobolev, V. I.; Kharitonov, A. S. The role of iron in N₂O decomposition on ZSM-5 zeolite and reactivity of the surface oxygen formed. *J. Mol. Catal.* **1990**, *61*, 85–97.

(17) Kulkarni, A. R.; Zhao, Z.-J.; Siahrostami, S.; Nørskov, J. K.; Studt, F. Cation-exchanged zeolites for the selective oxidation of methane to methanol. *Catal. Sci. Technol.* **2018**, *8*, 114–123.

(18) Mahyuddin, M. H.; Shiota, Y.; Yoshizawa, K. Methane selective oxidation to methanol by metal-exchanged zeolites: A review of active sites and their reactivity. *Catal. Sci. Technol.* **2019**, *9*, 1744–1768.

(19) Yuan, S.; Li, Y.; Peng, J.; Questell-Santiago, Y. M.; Akkiraju, K.; Giordano, L.; Zheng, D. J.; Bagi, S.; Román-Leshkov, Y.; Shao-Horn, Y. Conversion of methane into liquid fuels-bridging thermal catalysis with electrocatalysis. *Adv. Energy Mater.* **2020**, *10*, 2002154.

(20) Jisa, K.; Novakova, J.; Schwarze, M.; Vondrova, A.; Sklenak, S.; Sobalik, Z. Role of the Fe-zeolite structure and iron state in the N₂O decomposition: Comparison of Fe-FER, Fe-BEA, and Fe-MFI catalysts. *J. Catal.* **2009**, *262*, 27–34.

(21) Sklenak, S.; Andrikopoulos, P. C.; Boekfa, B.; Jansang, B.; Nováková, J.; Benco, L.; Bucko, T.; Hafner, J.; Dědeček, J.; Sobalik, Z. N₂O decomposition over Fe-zeolites: Structure of the active sites and the origin of the distinct reactivity of Fe-ferrierite, Fe-ZSM-5, and Fe-beta. A combined periodic DFT and multispectral study. *J. Catal.* **2010**, *272*, 262–274.

(22) Tabor, E.; Lemishka, M.; Sobalik, Z.; Mlekodaj, K.; Andrikopoulos, P. C.; Dedecek, J.; Sklenak, S. Low-temperature selective oxidation of methane over distant binuclear cationic centers in zeolites. *Commun. Chem.* **2019**, *2*, 71.

- (23) Dubkov, K. A.; Sobolev, V. I.; Panov, G. I. Low-temperature oxidation of methane to methanol on FeZSM-5 zeolite. *Kinet. Catal.* **1998**, *39*, 72–79.
- (24) Dubkov, K. A.; Paukshtis, E. A.; Panov, G. I. Stoichiometry of oxidation reactions involving alpha-oxygen on FeZSM-5 zeolite. *Kinet. Catal.* **2001**, *42*, 205–211.
- (25) Ivanov, D. P.; Sobolev, V. I.; Panov, G. I. Deactivation by coking and regeneration of zeolite catalysts for benzene-to-phenol oxidation. *Appl. Catal., A* **2003**, *241*, 113–121.
- (26) Yuranov, I.; Bulushev, D. A.; Renken, A.; Kiwi-Minsker, L. Benzene to phenol hydroxylation with N₂O over Fe-Beta and Fe-ZSM-5: Comparison of activity per Fe-site. *Appl. Catal., A* **2007**, *319*, 128–136.
- (27) Bols, M. L.; Hallaert, S. D.; Snyder, B. E. R.; Devos, J.; Plessers, D.; Rhoda, H. M.; Dusselier, M.; Schoonheydt, R. A.; Pierloot, K.; Solomon, E. I.; Sels, B. F. Spectroscopic identification of the alpha-Fe/alpha-O active site in Fe-CHA zeolite for the low-temperature activation of the methane C-H bond. *J. Am. Chem. Soc.* **2018**, *140*, 12021–12032.
- (28) Mlekodaj, K.; Dedecek, J.; Pashkova, V.; Tabor, E.; Klein, P.; Urbanova, M.; Karcz, R.; Sazama, P.; Whittleton, S. R.; Thomas, H. M.; Fishchuk, A. V.; Sklenak, S. Al organization in the SSZ-13 zeolite. Al distribution and extraframework sites of divalent cations. *J. Phys. Chem. C* **2019**, *123*, 7968–7987.
- (29) Sklenak, S.; Andrikopoulos, P. C.; Whittleton, S. R.; Jirglova, H.; Sazama, P.; Benco, L.; Bucko, T.; Hafner, J.; Sobalik, Z. Effect of the Al siting on the structure of Co(II) and Cu(II) cationic sites in ferrierite. A periodic DFT molecular dynamics and FTIR Study. *J. Phys. Chem. C* **2013**, *117*, 3958–3968.
- (30) Karcz, R.; Dedecek, J.; Supronowicz, B.; Thomas, H. M.; Klein, P.; Tabor, E.; Sazama, P.; Pashkova, V.; Sklenak, S. TNU-9 zeolite: Aluminum distribution and extra-framework sites of divalent cations. *Chem.—Eur. J.* **2017**, *23*, 8857–8870.
- (31) Dedecek, J.; Sobalik, Z.; Wichterlova, B. Siting and distribution of framework aluminium atoms in silicon-rich zeolites and impact on catalysis. *Catal. Rev. Sci. Eng.* **2012**, *54*, 135–223.
- (32) Dedecek, J.; Tabor, E.; Sklenak, S. Tuning the aluminum distribution in zeolites to increase their performance in acid-catalyzed reactions. *ChemSusChem* **2019**, *12*, 556–576.
- (33) Dedecek, J.; Lucero, M. J.; Li, C.; Gao, F.; Klein, P.; Urbanova, M.; Tvaruzkova, Z.; Sazama, P.; Sklenak, S. Complex analysis of the aluminum siting in the framework of silicon-rich zeolites. A case study on ferrierites. *J. Phys. Chem. C* **2011**, *115*, 11056–11064.
- (34) Dedecek, J.; Wichterlova, B. Co²⁺ ion siting in pentasil-containing zeolites. I. Co²⁺ ion sites and their occupation in mordenite. A Vis-NIR diffuse reflectance spectroscopy study. *J. Phys. Chem. B* **1999**, *103*, 1462–1476.
- (35) Sazama, P.; Tabor, E.; Klein, P.; Wichterlova, B.; Sklenak, S.; Mokrzycki, L.; Pashkova, V.; Ogura, M.; Dedecek, J. Al-rich beta zeolites. Distribution of Al atoms in the framework and related protonic and metal-ion species. *J. Catal.* **2016**, *333*, 102–114.
- (36) Dedecek, J.; Balgová, V.; Pashkova, V.; Klein, P.; Wichterlová, B. Synthesis of ZSM-5 zeolites with defined distribution of Al atoms in the framework and multinuclear MAS NMR analysis of the control of Al distribution. *Chem. Mater.* **2012**, *24*, 3231–3239.
- (37) Pickering, I.; Maddox, P. J.; Thomas, J. M.; Cheetham, A. K. A neutron powder diffraction analysis of potassium-exchanged ferrierite. *J. Catal.* **1989**, *119*, 261–265.
- (38) <http://www.iza-structure.org/databases> (accessed February 25, 2020).
- (39) Kresse, G.; Hafner, J. Ab-initio molecular-dynamics for open-shell transition-metals. *Phys. Rev. B: Condens. Matter Mater. Phys.* **1993**, *48*, 13115–13118.
- (40) Kresse, G.; Hafner, J. Ab-initio molecular-dynamics simulation of the liquid-metal amorphous-semiconductor transition in germanium. *Phys. Rev. B: Condens. Matter Mater. Phys.* **1994**, *49*, 14251–14269.
- (41) Kresse, G.; Furthmüller, J. Efficient iterative schemes for ab initio total-energy calculations using a plane-wave basis set. *Phys. Rev. B: Condens. Matter Mater. Phys.* **1996**, *54*, 11169–11186.
- (42) Kresse, G.; Furthmüller, J. Efficiency of ab-initio total energy calculations for metals and semiconductors using a plane-wave basis set. *Comput. Mater. Sci.* **1996**, *6*, 15–50.
- (43) Blöchl, P. E. Projector augmented-wave method. *Phys. Rev. B: Condens. Matter Mater. Phys.* **1994**, *50*, 17953–17979.
- (44) Kresse, G.; Joubert, D. From ultrasoft pseudopotentials to the projector augmented-wave method. *Phys. Rev. B: Condens. Matter Mater. Phys.* **1999**, *59*, 1758–1775.
- (45) Perdew, J. P.; Burke, K.; Ernzerhof, M. Generalized gradient approximation made simple. *Phys. Rev. Lett.* **1996**, *77*, 3865–3868.
- (46) Steinmann, S. N.; Corminboeuf, C. Comprehensive benchmarking of a density-dependent dispersion correction. *J. Chem. Theory Comput.* **2011**, *7*, 3567–3577.
- (47) Steinmann, S. N.; Corminboeuf, C. A generalized-gradient approximation exchange hole model for dispersion coefficients. *J. Chem. Phys.* **2011**, *134*, 044117.
- (48) Grimme, S. Accurate description of van der Waals complexes by density functional theory including empirical corrections. *J. Comput. Chem.* **2004**, *25*, 1463–1473.
- (49) Nosé, S. A unified formulation of the constant temperature molecular-dynamics methods. *J. Chem. Phys.* **1984**, *81*, 511–519.
- (50) Verlet, L. Computer “experiments” on classical fluids. I. Thermodynamical properties of Lennard-Jones molecules. *Phys. Rev.* **1967**, *159*, 98–103.
- (51) Verlet, L. Computer “experiments” on classical fluids. II. Equilibrium correlation functions. *Phys. Rev.* **1968**, *165*, 201–214.
- (52) Klein, P.; Dedecek, J.; Thomas, H. M.; Whittleton, S. R.; Pashkova, V.; Brus, J.; Kobera, L.; Sklenak, S. NMR crystallography of monovalent cations in inorganic matrixes: Li⁺ siting and the local structure of Li⁺ sites in ferrierites. *Chem. Commun.* **2015**, *51*, 8962–8965.
- (53) Sazama, P.; Moravkova, J.; Sklenak, S.; Vondrova, A.; Tabor, E.; Sadovska, G.; Pilar, R. Effect of the nuclearity and coordination of Cu and Fe sites in beta zeolites on the oxidation of hydrocarbons. *ACS Catal.* **2020**, *10*, 3984–4002.
- (54) Bultinck, P.; Van Alsenoy, C.; Ayers, P. W.; Carbó-Dorca, R. Critical analysis and extension of the Hirshfeld atoms in molecules. *J. Chem. Phys.* **2007**, *126*, 144111.